Two Dimensional Simplification of Complex Three Dimensional Wire Mesh Screens

Patrick N. Okolo[1,2], Kun Zhao[3], John Kennedy[4], Chigbo Mgbemena[5], Mkpamdi Eke[6], and Gareth J. Bennett[7]

[1]School of Engineering Computing and Mathematics, Oxford Brookes University, Oxford, OX33 1HX, UK. Email: pokolo@brookes.ac.uk

[2]Buildings Fluid Dynamics Limited, Dublin 2, Ireland: patrick.okolo@b-fluid.com

[3]Key Lab of Aerodynamic Noise Control, China Aerodynamics Research and Development Center, Mianyang, Sichuan, China, 621000. Email : kzhao@tcd.ie

[4]School of Engineering, Trinity College Dublin, the University of Dublin, Ireland. Email: kennedj@tcd.ie

[5]Department of Mechanical Engineering, University of Nigeria, Nsukka, Enugu 410001 Nigeria. Email: chigbo.mgbemene@unn.edu.ng

[6]Department of Mechanical Engineering, University of Nigeria, Nsukka, Enugu 410001 Nigeria. Email: mkpamdi.eke@unn.edu.ng

[7]School of Engineering, Trinity College Dublin, the University of Dublin, Ireland. Email: gareth.bennett@tcd.ie

ABSTRACT

This paper presents an approach to accurately characterise 3D wire screen geometries as simplified 2D screens for low Reynolds numbers. This is achieved by identifying 2D screen geometric features that provide appropriate approximations to a 3D realistic wire screen geometry. The simplified 2D screen geometries are obtained by varying geometric characteristics such as the streamwise pitch to diameter ratio within the range of $0 \leq \frac{C}{D} \leq 1$ for side by side cylinders. Both in-line and staggered cylinders with spanwise pitch to diameter ratios ranging from $2.94 \leq \frac{P}{D} \leq 5.56$

are examined here. A parametric study is performed for equivalent wire screen open area ratios varying within the range of $43.56\% \leq \beta \leq 67.26\%$. Numerical flow field comparisons between a 3D wire screen and its approximate 2D simplification are performed, with results further validated against NACA documented experiments. The equivalent 2D flow-loss coefficients agree very closely with the full 3D results, where for some Reynolds numbers, they are found to be within 6% of the NACA experimental results. Interestingly, both 2D and 3D results are found to under-predict the NACA values. The 2D results are also found to be much more accurate than well known flow correlations which are commonly used. 2D turbulence intensities measured at 570 diameters downstream of the screen were found to have the same values as the experimental results for some Reynolds numbers and were within 10% at worst. This demonstrates a real advantage over a 3D model where such a long numerical domain would be very computationally expensive. Out of-phase vortex shedding patterns exist for both in-line and staggered screen configurations in the range of $0 \leq \frac{C}{D} \leq 1$. The contribution of this work will enable design studies to examined for preliminary fast analysis of the effect of wire screens when applied as flow or noise control technologies.

INTRODUCTION

Wire mesh screens and perforated fairings are often utilized as fluid flow control mediums to reduce large-scale fluctuations (Mehta 1985), improve pressure uniformity, introduce or reduce turbulence and as a noise control method (Boorsma et al. 2009). More recently, the potential for wire screens to reduce aerodynamic broadband noise has been demonstrated. Of particular interest has been their efficacy at low to mid frequencies when applied to intricate parts of aircraft landing gears (Bouvy et al. 2016; Oerlemans et al. 2011; Smith et al. 2011). This research has led to higher Test Readiness Level (TRL) add-on technologies being developed and evaluated at full and large scale in coordinated test campaigns: (Bennett et al. 2018; Neri et al. 2018; Kennedy et al. 2016; Neri et al. 2015b; Neri et al. 2015a). The additional mass and size of these technologies need to be further studied from the perspective of their dynamics in order to prevent potential instabilities or "shimmy" of the landing gear as reported by (Eret et al. 2015).

In terms of fluid flow principles through a wire screen section, the screen introduces a pressure drop: Δp_c, velocity modification: V_c, turbulence alteration: T_c and also self-noise: N_c, the latter of which becomes predominant at high frequencies (Boorsma et al. 2009; Okolo et al. 2017).

The use of Computational Fluid Dynamics (CFD) to numerically resolve fluid flow through accurately modeled 3D wire screens often presents difficulties, because generating quality grids at regions of intersections between wire filament strands introduces complexities (Green et al. 2008; Okolo et al. 2019). Wire screens possess relatively small dimensions and features, thus possessing a very small contact surface region for streamwise flow. Creating the high-quality numerical grids required to accurately capture the boundary layers within this minimal contact region without employing advanced grid generation techniques becomes almost impossible (Valli et al. 2009). Therefore, in addition to the computational costs associated with performing 3D simulations, the added cost of generating grids of sufficient quality to properly capture the boundary layer flows makes this process much more expensive.

The open area ratio (Porosity) of wire screens can be calculated making use of Eq. 1

$$\beta = \frac{M^2}{(M+D)^2} \tag{1}$$

where β = open area ratio (porosity), D is the wire diameter and M is the open aperture mesh size.

Within this paper, an attempt is made to represent selected three-dimensional wire screens having open area ratios within $43.56\% \leq \beta \leq 67.26\%$, as approximate simplified 2D cylinders as shown in Fig. 1. P is the spanwise pitch distance, and C is the streamwise pitch distance.

3D to 2D simplification concept

Fig. 1 illustrates a number of 2D planar sectional views in the x-y plane where the streamwise pitch distance between cylinder pairs: 'C', varies between $\frac{C}{D} = 0$ from the wire screen (mesh) aperture centerline (P_{L1}), to $\frac{C}{D} = 1$ at the aperture edge (P_{L6}), as shown in Fig. 1 (b). Therefore, each x-y plane extracted from the 3D wire screen geometry is representative of a unique 2D cylinder arrangement possessing a distinct $\frac{C}{D}$ ratio. Therefore, by implication, 3D wire geometries

will shift from an approximate 2D cylinder in-line row arrangement at ($\frac{C}{D} = 0$) to a staggered row arrangement ($\frac{C}{D} = 1$). For fluid flow within a 3D (x-y-z) single wire screen aperture, a region of the fluid flow is in contact with the x-y surface located at plane (P_{L1}) where $\frac{C}{D} = 0$. Different fluid flow regions will be in contact with x-y surface of planes P_{L2}, P_{L3}, P_{L4}, P_{L5} and P_{L6}, and are therefore approximated accordingly within this paper. Thus, this parametric study replicates selected wire screens having open area ratios within the range $43.56\% \leq \beta \leq 67.26\%$. CFD results within this paper are validated against NACA documented experiments of Schubauer *et al.* (Schubauer, G.B and Spangenberg, W.G and Klebanoff, P.S 1950). The generation of a sufficiently detailed numerical mesh to fully capture the fluid mechanics of a wire screen of sub-millimetre filament diameter is still a significant computational challenge. This is all the more challenging when the wire screen is included in an analysis where much larger length scales are analysed such as the length of an aircraft. A 2D screen geometry as an approximation for the 3D wire screen would potentially aid fast turnaround CFD application analysis for studying the effect of flow control and noise reduction studies for various 2D aerodynamic shapes. This is potentially useful for practical applications, where the effect of wire screens could be obtained by using staggered cylinders as an approximate simplification. Proof of concept studies are often performed using approximate 2D aerodynamic shapes where both aerodynamics and noise studies are important. Khorrami *et al.* (Khorrami et al. 2007) carried out a NASA study, where simulations of flow interactions and aerodynamic airframe noise as well as wake interference between two cylinders in tandem configuration were performed in 2D CFD. Liu *et al.* (Liu et al. 2012) also performed 2D simulations on predictions of aerodynamic noise reduction of 2D circular cylinders by using open-cell metal foams as a low noise treatment strategy, where a hybrid method of coupling two-dimensional large eddy simulation (LES) with Ffowcs Williams Hawkings (FW–H) equation was utilized. Similarly, 2D simulations were carried out to study the effect of porous coatings on flow and noise control on tandem cylinder configurations (Liu et al. 2015). Therefore, this current research paper provides the possibility of studying the effect of wire screens (meshes) upstream or wrapped around 2D shapes for flow and noise control studies as it provides scientists and researchers with a tool towards performing

aerodynamic flow and noise control studies when using 2D wire screens.

In carrying out such approximate simplifications, a time saving but accurate approach is proposed to account for the physics of flows through selected wire screens with porosities in the range of $43.56\% \leq \beta \leq 67.26\%$ and for Reynolds numbers in the range of $42 \leq Re_D \leq 250$.

Within this current paper, the Re_D (Reynolds number based on wire screen diameter) is based upon the wire screen filament diameter: diameters in the range of $0.19x10^{-3}m$ to $0.43x10^{-3}m$, this means that the Reynolds numbers are extremely low compared to the more commonly reported Reynolds numbers for Landing Gear applications when it is the wheel diameter which is used as the length reference.

For flows past cylinder pairs, vortex shedding patterns have been shown to largely depend on a characteristic spacing, i.e, the spanwise pitch to diameter ratio $\frac{P}{D}$ as reported by (Williamson 1996; Asghar and Jumper 2009), where the vortex shedding between cylinder pairs predominantly exist in a 180° out-of-phase pattern or an in-phase pattern as depicted by Fig. 2.

BACKGROUND THEORY

Flow Loss Coefficient

Equation 2 shows the conventional non-dimensional relationship between the flow loss coefficient, the static pressure drop, and the dynamic pressure

$$K = \frac{\Delta p}{0.5\rho U_\infty^2} \tag{2}$$

where K is the flow loss coefficient, Δp the static pressure drop across the screen, ρ the fluid density, and U_∞ the free stream velocity. Empirical correlations of flow loss coefficient through single screens have been well documented: (Pinker and Herbert 1967; Wieghardt 1953; Roach 1987; Wakeland and Keolian 2003), and such correlations are generally based on wire diameter and open area ratio. They generally take the form of Eq. 3;

$$K = G(\beta)\left(\frac{Z_1}{Re_D} + Z_2\right) \tag{3}$$

Where G is only a function of β, while Z_1 and Z_2 are correlation constants and Re_D is the Reynolds number based on the wire diameter. Frequently used G function variants have been documented by (Pinker and Herbert 1967). For the choice of Reynolds number, two different velocities can be used; the free-stream approach velocity U_∞ or approximate local velocity through the screen aperture $U_s = \frac{U_\infty}{\beta}$.

Screen Turbulence Reduction

Wire screens have been found to alter the turbulence characteristics of fluids as a function of the flow loss coefficient (K) as documented by (Dryden 1947; Groth and Arne 1988; Krogstad and Davidson 2011). Within the near field of the downstream wake region of screens, the flow exits in an anisotropic turbulent form with much higher turbulence intensities than to be found upstream. However, at over 20 wire diameters downstream of the screen, the turbulence becomes isotropic as shown by the experimental investigations of (Groth and Arne 1988). (Batchelor and Townsend 1948a; Batchelor and Townsend 1948b) highlighted the decay of anisotropic turbulence within the initial and final decay periods, thus resulting in the knowledge that a decay region exists further downstream, where anisotropic intensities reduce rapidly and turbulence returns to a near-isotropic state.

The damping factor introduced by a wire screen into a flow field is expressed as the ratio of turbulence intensity produced at a location after the fluid stream passes through the screen to the turbulence intensity at the same location but with the wire screen absent, depicted by Eq. 4.

$$f_u = \frac{(u'_{rms})_{screen_{(present)}}}{(u'_{rms})_{screen_{(absent)}}}, \quad f_v = \frac{(v'_{rms})_{screen_{(present)}}}{(v'_{rms})_{screen_{(absent)}}} \tag{4}$$

Where f_u is the axial turbulence reduction factor, f_v the lateral turbulence reduction factor, u'_{rms} the rms velocity perturbation in axial direction, and v'_{rms} the rms velocity perturbation in lateral direction. The axial and lateral damping factors can be distinguished for screens and are expected to be markedly different within the initial anisotropic turbulent region, but as turbulence returns to an isotropic state downstream, axial and lateral turbulence reduction factors almost become

indistinguishable. Prandtl (Prandtl 1933) proposed Eq. 5 in 1933, with Collar (Collar 1939) (Eq. 6), Dryden (Dryden 1947) (Eq. 7) and Taylor *et al.* (Taylor et al. 1949) (Eq. 8) proposing alternatives in subsequent studies.

$$f_u = \frac{1}{1+K} \tag{5}$$

$$f_u = \frac{2-K}{2+K} \tag{6}$$

$$f_u = \frac{1}{\sqrt{1+K}} \tag{7}$$

$$f_u = \frac{1+\alpha-\alpha K}{1++\alpha+K}\,, \quad f_v = \alpha \tag{8}$$

Where α is the ratio of the flow angle of incidence with respect to the normal to the screen surface for the upstream flow, to the angle of incidence for the downstream flow.

(Kistler and Vrebalovich 1966) performed measurements of grid turbulence for flows with high Reynolds numbers ranging from $1.2 \times 10^5 \leq Re_D \leq 2.4 \times 10^6$, and results showed that no new phenomenon was introduced for high Reynolds number flows through screen grids. As such, experiments of low Reynolds number flows were adequate to describe the main features of turbulent flow phenomenon through wire screen grids.

For the pressure loss coefficient of wire screens, documented studies have shown that the decay function of Re_D is dependent on the Reynolds number based on wire screen diameter. (Roach 1987) presented a collection of literature data and showed that for this decay when Reynolds number is $Re_D < 10$, decay Re_D^{-1}, which is characteristic for laminar flow through the wire screens. For Re_D larger than about 40, vortex shedding starts around the wires and the behaviour of the decay changes. For intervals of $40 < Re_D > 105$, the decay occurs faster as $Re_D^{4/3}$, and this decay asymptotically approaches a constant value of 0.52 in the limit of high Re_D, (Roach 1987; Kurian

and Fransson 2009). This further highlights the experimental work of (Kistler and Vrebalovich 1966), that the decay spectral shapes at small wave number is independent of Reynolds number based on wire diameter Re_D, and as such, data taken at low Re_D is sufficient to describe the pressure loss as a decay function of Re_D. The decay function of Re_D phenomenon at low Re_D is similar to that at high Re_D (40 <Re_D>105), and hence no new phenomenon is introduced with regards to the decay function of Re_D.

Therefore, although the numerical simulations performed within this present paper are for low Reynolds number range of $42 \leq Re_D \leq 250$, it is believed that the flow phenomenon within this range is sufficient enough for the scope and aims of the paper.

NUMERICAL SETUP

In order to validate the approach, numerical simulations were conducted on 3D wire screen geometries and compared to results from the approximated 2D model simulations. Screen geometric details are highlighted in Table 1. Initial tests for grid sensitivity and the turbulence model selection were conducted followed by calculations of the flow loss coefficients using a steady RANS approach. Following this, studies of the vortex shedding patterns and unsteady flow speeds were performed using a time-averaged Unsteady-RANS approach.

Computations were carried out on a single node-24 core grid platform, with a runtime for each 2D case taking an average of 120 mins, in contrast to 840 mins average runtime for the 3D simulations. Therefore, 2D simulations were an average of 7 times faster than the 3D simulation cases. Simulation runtime comparison for 2D vs 3D cases are as in Table 2.

Wire Screen Test-Cases

Details and dimensions of the wire screen models examined for the numerical analysis carried out within this study are presented in this subsection.

2D Screen Geometric Characteristics

A generalized row of six cylinders where the center to center relative displacements are shown in Fig. 2 (c) is numerically analysed. The geometric properties of the cylinders are as shown in

Table 1. In addition, simulations were conducted as a function of the streamwise dimension 'C' in the range $0 \leq \frac{C}{D} \leq 1$, with increments of 0.2. It is pointed out here that the geometries of the screen models in Table 1 were chosen to replicate those of the real wire screens (four selected screens) experimentally tested in the work of Schubauer *et al.* (Schubauer, G.B and Spangenberg, W.G and Klebanoff, P.S 1950), which enables validation of the numerical method within this paper.

3D Screen Geometry Model

In order to compare the approximate 2D simplifications to the full 3D models, 3D wire screen models with a geometry as previously shown in Figure 1 (a), and having geometric specifications of diameter and porosity as shown in Table 1 are also analyzed.

Numerical Grid Generation and Boundary Conditions

Numerical grid generation is carried out using the ANSYS ICEM meshing software. Examples of the 2D and 3D numerical grids used are shown in Fig. 3 illustrating also the applied boundary conditions. Velocity inlet and pressure outlet conditions were applied as shown. Slip wall conditions (i.e. no shear stress or flow-through) were applied at the top, bottom and side boundaries, while the cylinders themselves had no-slip wall boundary conditions. Domain sizes are also shown in Fig. 3, where $L_y \geq 30D$ for the 2D screen cases, and L_x is as shown.

The numerical grid for the three-dimensional screen sample has boundary sides which are flush with the edges of the wire screens, as the wire screen is tightly fitted within the flow channel with slip wall conditions employed as boundary conditions for all sides (zero shear stress and zero flow-through). The 3D wire mesh screen itself also had a no-slip wall boundary condition. Values of average $y+$ of less than one were maintained at the wire screen walls at all times. Numerical grid fluid domain extensions are also as shown in Fig. 3. For the 3D wire screen, 4x4 apertures were modeled in order to generate a numerical grid of sufficient quality. A gap size of less than 5% of D was introduced at screen wire strand intersection points, as without these gaps the intersections often resulted in poor grid cell skewness and very low-quality meshing within this region which subsequently produced poor CFD code convergence and results. Previous studies carried out by Green ((Green et al. 2008)) had shown that such small gaps at intersections had a very minimal

effect on overall CFD results and the flow speeds through such gaps were very negligible compared to flow speeds through the screen apertures.

Grid Sensitivity and Discretization Error

Results of grid independence studies and discretization error estimates when the $k-\omega$ turbulence model was used for the 2D screen (screen sample 4), and the $k-\epsilon$ model for the 3D screen (screen sample 4), is presented in Fig.4 and summarized in Table 3. The widely accepted GCI (Grid Convergence Index) discretization error method is utilized. The GCI approach is based on the Richardson Extrapolation (RE) method, and this method has shown to be a reliable method for discretization errors for a wide array of CFD simulation cases (Roache 1994; Roache 1997). The GCI of static pressure drop for the 2D case was 5.6%, while the GCI for the 3D simulation case was 5.5%. These GCI values fall within the acceptable range, hence the discretization errors within the numerical code are acceptable. Based on these studies, cell numbers of approximately 1.3 million were used for the 2D screen grid, while a cell number of 6 million was used for the 3D wire screen grid.

Turbulence Model Selection Study

The turbulence model selection study was carried out for 2D screens on screen sample 4 for an in-line screen arrangement ($C/D = 0$). The laminar model, standard $k-\epsilon$, Re- Normalisation Group (RNG) $k-\epsilon$, realizable $k-\epsilon$, standard $k-\omega$ and Shear Stress Transport (SST) $k-\omega$ turbulence models were used as test studies in order to capture the flow through the screen configurations ($C/D = 0$) at different Reynolds numbers. Results of the mean static pressure drop across the screens compared to the experimental results of Schubauer *et al.* (Schubauer, G.B and Spangenberg, W.G and Klebanoff, P.S 1950) are presented in Fig. 5 (a).

As seen from Fig. 5 (a), the laminar model performs closely to experiments for the 2D case, and this is comparable to the laminar model performance in Fig. 5 (b) for the 3D cases. However, the exclusive use of a laminar flow model to simulate the 2D or 3D cases will not enable additional analysis for isotropic turbulence reduction parameters (isotropic turbulent kinetic energy) which is one of the main benchmark parameters needed to calculate the turbulence intensities and resulting

turbulence reductions. Apart from the laminar model, the $k-\omega$ turbulence model provides the most reflective comparison to experiment, hence this turbulence model was utilized for all subsequent analysis of 2D screens with low Reynolds number corrections and production limiter.

The SIMPLE pressure-velocity coupling scheme was utilized, with least squares cell-based gradient spatial discretization, second-order discretization for pressure, second-order upwind discretization for momentum, turbulent kinetic energy, and specific dissipation rate. A pressure under-relaxation factor of 0.2 was utilized, with values of 0.5 chosen for momentum, 0.6 for turbulent kinetic energy and 0.6 for specific dissipation rate. A value of $y+ \approx 1$ was maintained on all screen surfaces, and the time-step for unsteady analysis was such as produced average CFL number of less than one for all grids, and which also resulted in having a minimum of 50 period cycles per time-step based on a cylinder Strouhal number of 0.2. A turbulence intensity at each inlet boundary condition was chosen to match those measured in the NACA experiments. Therefore, according to the experimental results, inlet turbulence intensities of within 0.7%, 0.8% and 1% were sufficient for the CFD simulations.

Equally, a turbulence model selection study for the 3D wire screen case is as presented in Fig. 5 (b), with the standard $k-\epsilon$ model found to be best able to replicate the experimental results.

THE 3D AND 2D VELOCITY FIELD COMPARISON

In order to show that two-dimensional wire screens (cylinder arrangements) can serve as approximations / simplifications to three-dimensional wire screens, comparisons were carried out between 3D wire screen averaged velocity flow field results and 2D screen mean flow field results as shown in Fig. 6. To present the 3D flow results, x-y surface areas of planes P_{L1}, P_{L2}, P_{L3}, P_{L4}, P_{L5} and P_{L6} are used to present the velocity contour plots along the planes which correspond to particular $\frac{C}{D}$ ratios of equivalent 2D circular cylinders. Each plane extracted from the 3D wire screen result corresponds to a unique 2D geometric configuration having an equivalent $\frac{C}{D}$ ratio to the 3D wire screen case. From the results of Fig. 6, it can be observed that a similar and comparable flow field through the screen arrangement exists between the 3D wire screen and a simplified 2D screen arrangement when the ratio of $\frac{C}{D}$ is adjusted between $0 \leq \frac{C}{D} \leq 1$. This agreement is best up

to $\frac{C}{D} = 0.6$, where the maximum flow speeds through the 3D wire screen aperture are comparable to those through the equivalent 2D cylinder arrangement. In this range, the measured flow speed differences between the 3D and 2D screen cases are between 4% to 14%. However, within the range of $0.8 \leq \frac{C}{D} \leq 1$, flow speed differences of up to 30% are calculated. An explanation for the relatively poor comparison between the 3D and 2D cases within this range is due to the effect of the adjacent screen wire filament strands (the weft). The proximity of this surface in the 3D model causes a boundary layer to form, thus retarding the flow and reducing the velocity close to the weft wire at $\frac{C}{D} = 1$. Therefore, from the 3D and 2D flow field velocity comparisons carried out, it is observed that within the range of $0 \leq \frac{C}{D} \leq 0.6$, the flow field through 2D simplified cylindrical screen arrangements are comparable to flow fields through 3D wire screens. Hence, using a 2D cylindrical arrangement as a simplification to 3D wire screens will be the focus of subsequent sections within this paper.

WIRE SCREEN RESULTS

Results of the instantaneous vortex shedding patterns, mean velocity field, flow loss coefficient and turbulence reduction factors from the two-dimensional screens are presented in this section.

2D Vortex Shedding Phase Patterns

Flow regimes of interest for fluid flow past screen sample 1 lies within the turbulence transition range for vortex street being within $150 \leq Re_D \leq 300$, while flow regimes of screen samples 2, 3 and 4 are located within the two regime wake where a vortex street exists in a laminar and clearly alternating $40 \leq Re_D \leq 150$ form (Lienhard 1966). Instantaneous fluctuating flow fields showing vortex shedding patterns were analyzed for 2D screen samples tested, where patterns for screen sample 4 having $P/D = 5.56$ presented as instantaneous vorticity magnitude contours are shown in Fig 7 and instantaneous unsteady velocity streamlines as shown in Fig. 8. Within the range of $0 \leq \frac{C}{D} \leq 1$ tested, it was observed than cylinders possessing an in-line configuration $\frac{C}{D} = 0$ produced vortex shedding from adjacent cylinders that were predominantly out of phase, which is rightly expected for the range of P/D tested, e.g $P/D = 5.56$ for screen sample 4, where weak interaction between adjacent cylinders exists only slightly. The same trend can be observed to exist

when the screen geometric configuration changes, i.e within $0 \leq \frac{C}{D} \leq 1$, where predominantly out of-phase vortex shedding pattern exists for pairs of adjacent cylinders. Results of vortex shedding patterns of screen samples 1, 2 and 3 showed similar behaviors.

Streamlines of mean velocity within the wake region of the 2D cylinder arrangement for screen sample 4 is presented in Fig. 9, where mean field calculations are achieved after a fully developed unsteady flow field. Streamlines within the wake region of cylinder arrangements for a range $0 \leq C/D \leq 1$ are presented, and these follow patterns expected of mean flow fields.

Flow Loss Coefficient

Numerical results of the screen flow loss coefficient for the 2D simplified screens are compared with 3D results and benchmarked against documented NACA experiments carried out by Schubauer *et al.* (Schubauer, G.B and Spangenberg, W.G and Klebanoff, P.S 1950). Results of flow loss across screens are presented in Fig. 10.

As screen geometric characteristics switch from an in-line geometry $C/D = 0$ to an off-line staggered geometry $0 < \frac{C}{D} \leq 1$, varying results of flow loss coefficients are obtained for the same flow conditions. It is observed that the trend for the flow loss coefficients for both the 3D and 2D simulations compare very well with the experimental results. The 3D simulation agrees best for all cases but despite that the 2D simplification provides a good approximation being best within the range $0.4 \leq \frac{C}{D} \leq 0.6$. At $C/D = 0.4$, the best flow loss coefficient agreements of up to -5.1% were achieved for screen 1, -7.3% for screen 2, -9.6% for screen 3 and -4.9% for screen 4. 3D results compared within -6% of the experiment, and in general, 2D results under-predicted more than 3D results when compared to experimental values due to the difference in pressure drop.

Comparisons between the CFD flow loss coefficient results and some existing flow loss prediction correlations were also carried out as presented in Fig. 11. The P_{L3} screen geometry, $C/D = 0.4$ was used for this comparison. Taking screen sample 3 as an illustration, the Wakeland *et al.* (Wakeland and Keolian 2003) correlation over predicted up to 20.4% compared to experiments, the Wieghardt (Wieghardt 1953) correlation over-predicted by 17.1%, the Roach correlation over-predicted by 23%, while 2D CFD under-predicted by a worst case of -12.2%, and 3D showed

to under-predict by -5%. Therefore, taking these compared predictions into consideration, it is observed that the 2D screens CFD prediction approach presents a better comparison to experiments when compared to existing classical correlation prediction models within the range of Reynolds number tested, and can serve as good approximations to 3D model cases.

Turbulence Intensity Reduction

2D axial turbulence intensity results were obtained at a distance of 556D downstream for screen sample 4, and this is as presented in Fig. 12. Due to length scales involved for the measurement location, measurement of turbulence parameters for a 3D case at 556D downstream would have been highly time consuming. Within the range of Reynolds number tested for the 2D cases, axial turbulence was predicted to within $\pm 10\%$ error compared to the experimental values. In this case, screen geometric configurations within $0.4 \leq \frac{C}{D} \leq 0.6$ yielded only marginally better comparisons when compared to other configurations. The figure is very significant as it demonstrates that far-field downstream turbulence CFD results can very accurately replicate complicated experiments with just a simple 2D analysis.

As discussed, the turbulence behavior far downstream of wire screens is expected to be isotropic in nature, where the decay of progressive turbulence could be regarded as an isotropic decay. Therefore, comparisons between 2D turbulence reductions and isotropic turbulence reduction factor models are carried out and results presented in Fig. 13. The turbulence reduction factor relations (Prandtl 1933; Collar 1939; Dryden 1947) are compared with the CFD predicted axial component of turbulence reduction factors. As shown in Fig. 13, results for screen samples show best agreement with the (Dryden 1947) component of turbulence reduction factors. As documented in Schubauer *et al.* (Schubauer, G.B and Spangenberg, W.G and Klebanoff, P.S 1950), experiments also showed best agreement with the (Dryden 1947) model. Hence, we observe and conclude that CFD predicted reduction factors from a 2D simplified screen compares well with reduction factors using the (Dryden 1947) model, which also followed documented experimental observations.

CONCLUSIONS

In this paper, studies are carried out to characterize selected 3D wire screens as approximate simplified 2D screen geometry configurations. This parametric study examines wire screens having open area ratios within the range $43.56\% \leq \beta \leq 67.26\%$. For this study, three key 2D case vs 3D case comparisons (velocity flow field comparison, pressure loss comparison and turbulence reduction comparison) are used to compare and investigate the C/D variation for a 2D screen $0 \leq \frac{C}{D} \leq 1$ compared to a 3D case while specifically benchmarking these results against NACA documented experiments. For the velocity flow fields comparison, the 2D vs 3D flow field velocity comparisons showed that within the range of $0 \leq \frac{C}{D} \leq 0.6$, the flow field through 2D simplified screen are most comparable to flow fields through 3D wire screens. A look into the pressure loss comparisons show that although the 3D case flow loss agrees better to experiments, yet, the 2D simplification provides a good approximation when within $0.4 \leq \frac{C}{D} \leq 0.6$ range. More specifically, when $C/D = 0.4$, the flow loss coefficient agrees to experiment by up to -5.1% for screen 1, -7.3% for screen 2, -9.6% for screen 3 and -4.9% for screen 4. Results of the 3D and 2D cases all had a general trend of underpredicting flow loss coefficient when compared to experiments, however the 2D mesh screen 3 case underpredicted slightly more than the other screen cases, hence, screen 3 results gave higher percentage error when compared to other screens. A possible reason for this is seen from the flow field results where mesh screen 3 showed to slightly underpredict particularly more pressure loss and turbulence kinetic energy when compared to other screen cases. The underprediction of screen 3 when compared to other 2D screen cases did not have a correlated trend with their screen geometric features (e.g, screen diameter, streamwise & spanwise pitch, porosity, or solidity).

The turbulence effect comparison showed that within the range of Reynolds number (Re_D) tested, 2D case axial turbulence predicted to within $\pm 10\%$ error compared to experimental values. Again, from these results, screen geometric configurations within $0.4 \leq \frac{C}{D} \leq 0.6$ yielded marginally better comparisons when compared to other configurations. Hence, from these key comparisons, the 2D simplification provides a good approximation when within $0.4 \leq \frac{C}{D} \leq 0.6$ range, or to be specific, when $C/D = 0.4$. A physical explanation to this result can be linked to the fact that within

388 $0.4 \leq \frac{C}{D} \leq 0.6$, the 2D screen configuration better mimics a 3D screen geometry in the planar view
389 as seen in Figure 1 pictorial explanation and all resulting plots. When this mimic situation occurs,
390 then resulting flow speeds, loss coefficients and turbulence characteristics of a 3D wire screen are
391 well replicated in its 2D equivalent. Therefore, 3D vs 2D wire screen comparisons performed
392 showed that 2D screens could serve as simplified approximations for 3D wire screens, with similar
393 wake velocity fields achievable and agreeing to within 4% to 14% in the range of $0 \leq \frac{C}{D} \leq 0.6$.
394 For 2D cylindrical geometries possessing in-line and staggered arrangements, i.e, $0 \leq \frac{C}{D} \leq 1$, out-
395 of-phase vortex shedding patterns exists within the wake region. The level of isotropic turbulence
396 downstream of a screen is predicted by the simplified 2D screen, and comparisons of CFD turbulence
397 reduction to existing relations equally showed realistic agreements. Hence for wire screens, 2D
398 modeling of the flow physics within the range $0.4 \leq \frac{C}{D} \leq 0.6$ represents a favourable interpretation
399 and simplification for a 3D wire screen. This geometry range is hereby recommended for use
400 in applications and analysis involving 2D shapes where flow and or noise control studies are of
401 significance.

402 **DATA AVAILABILITY**

403 Some or all data, models, or code that support the findings of this study are available from the
404 corresponding author upon reasonable request.

405 **ACKNOWLEDGEMENTS**

406 The research leading to these results received funding from the European Union's Seventh
407 Framework Programme (FP7/2007-2013) for the Clean Sky Joint Technology Initiative under grant
408 agreements number [308225] (ALLEGRA) and number [620188] (ARTIC). The authors also thank
409 the Irish Center for High-End Computing (ICHEC) for allowing access to their supercomputers for
410 the computations performed within this research study.

411 **REFERENCES**

412 Asghar, A. and Jumper, E. J. (2009). "Phase synchronization of vortex shedding from two circular
413 cylinders using plasma actuators." *AIAA Journal*, 47(7), 1608–1616.

Batchelor, G. K. and Townsend, A. A. (1948a). "Decay of Isotropic Turbulence in the Initial Period." *Proceedings of the Royal Society A: Mathematical, Physical and Engineering Sciences*, 193(1035), 539–558.

Batchelor, G. K. and Townsend, A. A. (1948b). "Decay of Turbulence in the Final Period." *Proceedings of the Royal Society A: Mathematical, Physical and Engineering Sciences*, 194(1039), 527–543.

Bennett, G. J., Neri, E., and Kennedy, J. (2018). "Noise characterization of a full-scale nose landing gear." *Journal of Aircraft*, 1–37.

Boorsma, K., Zhang, X., Molin, N., and Chow, L. C. (2009). "Bluff body noise control using perforated fairings." *AIAA Journal*, 47(1), 33–43.

Bouvy, Q., Petot, B., and Rougier, T. (2016). "Review of landing gear acoustic research at messier-bugatti-dowty." *22nd AIAA/CEAS Aeroacoustics Conference*, American Institute of Aeronautics and Astronautics (May).

Collar, A. R. (1939). *The effect of a gauze on the velocity distribution in a uniform duct*. British Aeronautical Research Council, London.

Dryden, H. L. (1947). "The use of damping screens for the reduction of wind-tunnel turbulence." *Journal of the Aeronautical Sciences*, 14(4), 221–228.

Eret, P., Kennedy, J., and Bennett, G. J. (2015). "Effect of noise reducing components on nose landing gear stability for a mid-size aircraft coupled with vortex shedding and freeplay." *Journal of Sound and Vibration*, 354, 91–103.

Green, S. I., Wang, Z., Waung, T., and Vakil, A. (2008). "Simulation of the flow through woven fabrics." *Computers & Fluids*, 37(9), 1148–1156.

Groth, J. and Arne, J. (1988). "Turbulence reduction by screens." *Journal of Fluid Mechanics*, 197(-1), 139.

Kennedy, J., Neri, E., and Bennett, G. J. (2016). "The reduction of main landing gear noise." *22nd AIAA/CEAS Aeroacoustics Conference*, Lyon, France.

Khorrami, M. R., Choudhari, M. M., Lockard, D. P., Jenkins, L. N., and Mcginley, C. B. (2007).

"Unsteady Flowfield Around Tandem Cylinders as Prototype Component Interaction in Airframe Noise." *AIAA Journal*, 45(8), 1930–1941.

Kistler, A. L. and Vrebalovich, T. (1966). "Grid turbulence at large Reynolds numbers." *Journal of Fluid Mechanics*, 26(01), 37.

Krogstad, P. and Davidson, P. A. (2011). "Freely decaying, homogeneous turbulence generated by multi-scale grids." *Journal of Fluid Mechanics*, 680, 417–434.

Kurian, T. and Fransson, J. H. M. (2009). "Grid-generated turbulence revisited." *Fluid Dynamics Research*, 41(2), 021403 Publisher: IOP Publishing.

Lienhard, J. (1966). "Synopsis of lift, drag and vortex frequency data for rigid circular cylinders.." *Washington State University College of Engineering Research Division Bulletin 300:3*, Pullman, Wash. : Technical Extension Service, Washington State University.

Liu, H., Azarpeyvand, M., Wei, J., and Qu, Z. (2015). "Tandem cylinder aerodynamic sound control using porous coating." *Journal of Sound and Vibration*, 334, 190–201.

Liu, H., Wei, J., and Qu, Z. (2012). "Prediction of aerodynamic noise reduction by using open-cell metal foam." *Journal of Sound and Vibration*, 331(7), 1483–1497.

Mehta, R. D. (1985). "Turbulent boundary layer perturbed by a screen." *AIAA Journal*, 23(9), 1335–1342.

Neri, E., Kennedy, J., and Bennett, G. (2018). "Bay cavity noise for full-scale nose landing gear: A comparison between experimental and numerical results." *Aerospace Science and Technology*, 72, 278–291.

Neri, E., Kennedy, J., and Bennett, G. J. (2015a). "Aeroacoustic source separation on a full scale nose landing gear featuring combinations of low noise technologies." *ASME 2015 Noise Control and Acoustics Division Conference at InterNoise 2015*, American Society of Mechanical Engineers, San Francisco, California, USA.

Neri, E., Kennedy, J., and Bennett, G. J. (2015b). "Characterization of low noise technologies applied to a full scale fuselage mounted nose landing gear." *ASME 2015 Noise Control and Acoustics Division Conference at InterNoise 2015*, American Society of Mechanical Engineers,

San Francisco, California.

Oerlemans, S., Sandu, C., Molin, N., and Piet, J.-F. (2011). "Reduction of landing gear noise using meshes." *16th AIAA/CEAS Aeroacoustics Conference*, American Institute of Aeronautics and Astronautics.

Okolo, P. N., Zhao, K., Kennedy, J., and Bennett, G. J. (2017). "Numerical Modeling of Wire Screens for Flow and Noise Control." *23rd AIAA/CEAS Aeroacoustics Conference*, American Institute of Aeronautics and Astronautics.

Okolo, P. N., Zhao, K., Kennedy, J., and Bennett, G. J. (2019). "Numerical assessment of flow control capabilities of three dimensional woven wire mesh screens." *European Journal of Mechanics - B/Fluids*, 76, 259 – 271.

Pinker, R. A. and Herbert, M. V. (1967). "Pressure loss associated with compressible flow through square-mesh wire gauzes." *ARCHIVE: Journal of Mechanical Engineering Science 1959-1982 (vols 1-23)*, 9(1), 11–23.

Prandtl, L. (1933). *Attaining a steady air stream in wind tunnels*. NACA TM 726.

Roach, P. (1987). "The generation of nearly isotropic turbulence by means of grids." *International Journal of Heat and Fluid Flow*, 8(2), 82–92.

Roache, P. J. (1994). "Perspective: A Method for Uniform Reporting of Grid Refinement Studies." *Journal of Fluids Engineering*, 116(3), 405.

Roache, P. J. (1997). "Quantification of uncertainty in computational fluid dynamics." *Annual Review of Fluid Mechanics*, 29(1), 123–160.

Schubauer, G.B and Spangenberg, W.G and Klebanoff, P.S (1950). "Aerodynamic characteristics of damping screens." *Report No. NACA TN 2001*, NACA.

Smith, M., Chow, L. C., and Molin, N. (2011). "Control of landing gear noise using meshes." *16th AIAA/CEAS Aeroacoustics Conference*, 3974.

Taylor, G. I., Batchelor, G. K., Dryden, H. L., and Schubauer, G. B. (1949). "The effect of wire gauze on small disturbances in a uniform stream." *The Quarterly Journal of Mechanics and Applied Mathematics*, 2(1), 1–29.

Valli, A., Hyväluoma, J., Jäsberg, A., Koponen, A., and Timonen, J. (2009). "Pressure Drop for Low Reynolds-Number Flows Through Regular and Random Screens." *Transport in Porous Media*, 80(2), 193–208.

Wakeland, R. S. and Keolian, R. M. (2003). "Measurements of resistance of individual square-mesh screens to oscillating flow at low and intermediate reynolds numbers." *Journal of Fluids Engineering*, 125(5), 851.

Wieghardt, K. E. G. (1953). "On the resistance of screens." *Aeronautical Quarterly*, 4(02), 186–192.

Williamson, C. (1996). "Vortex dynamics in the cylinder wake." *Annual Review of Fluid Mechanics*, 28(1), 477–539.

List of Tables

TABLE 1. Geometric Characteristics of Screen Samples

Screens Tested				
Sample	D (mm)	P (mm)	P/D	β (%)
1	0.43	1.27	2.94	43.56
2	0.14	0.47	3.36	49.38
3	0.18	0.64	3.57	51.84
4	0.19	1.06	5.56	67.26

TABLE 2. Average Simulation Runtime

	2D Screen ($0 \leq \frac{C}{D} \leq 1$)	3D Screen
Sample 1	118.4 mins	841.2 mins
Sample 2	121.2 mins	836.5 mins
Sample 3	122.1 mins	844.1 mins
Sample 4	199.5 mins	839.4 mins

TABLE 3. Grid Independence Study: Screen 4 (Re_D = 120). Cells (10^6), and ΔP (Pa)

	2D Screen		3D Screen	
	Cells	ΔP	Cells	ΔP
1	0.2	22.2	1.1	25.1
2	0.6	26.9	2.6	31.2
3	1.3	28.8	4.0	32.1
4	1.6	29.4	6.0	33.5
5	2.0	29.7	7.8	33.9
ϕ_{ext}		30.43		34.9
e_{ext}		4.3%		4.2%
GCI_{fine}		5.6%		5.5%

List of Figures

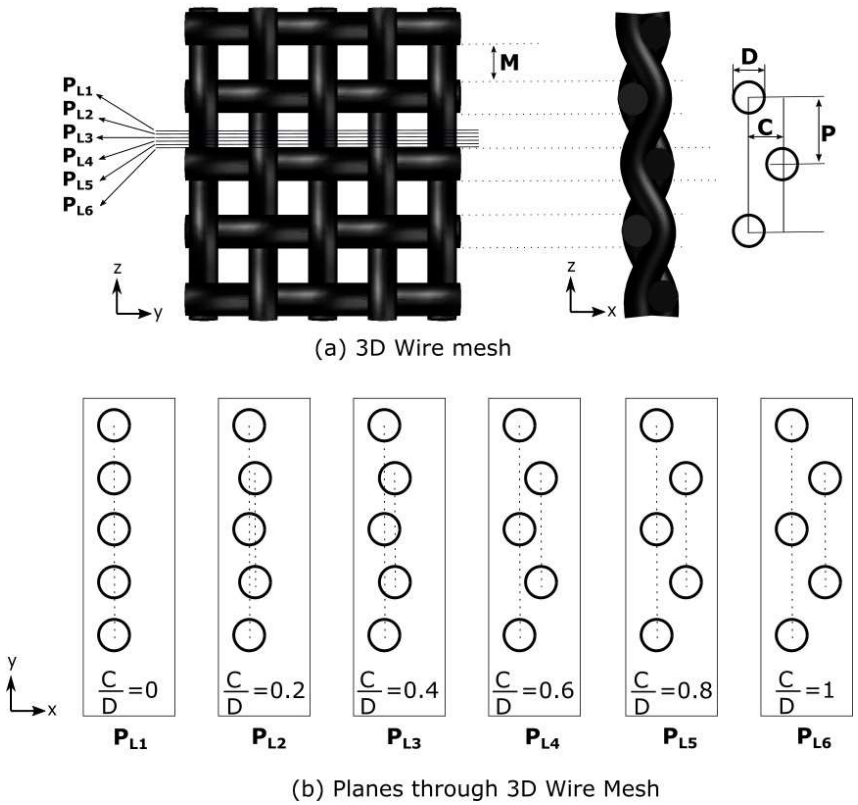

Fig. 1. Wire Screen (mesh)

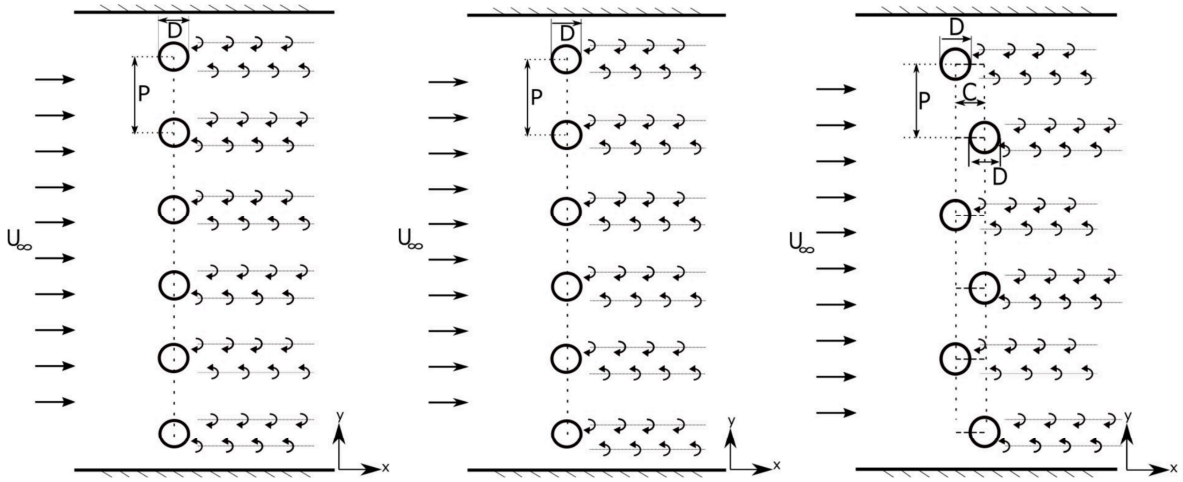

(a) Out of Phase Pattern $2 \leq \frac{P}{D} \leq 6$ (b) In-Phase Pattern $\frac{P}{D} > 6$ (c) $0 \leq \frac{C}{D} \leq 1$ and $2 \leq \frac{P}{D} \leq 6$

Fig. 2. Phase pattern of vortex shedding in the wake of cylinders

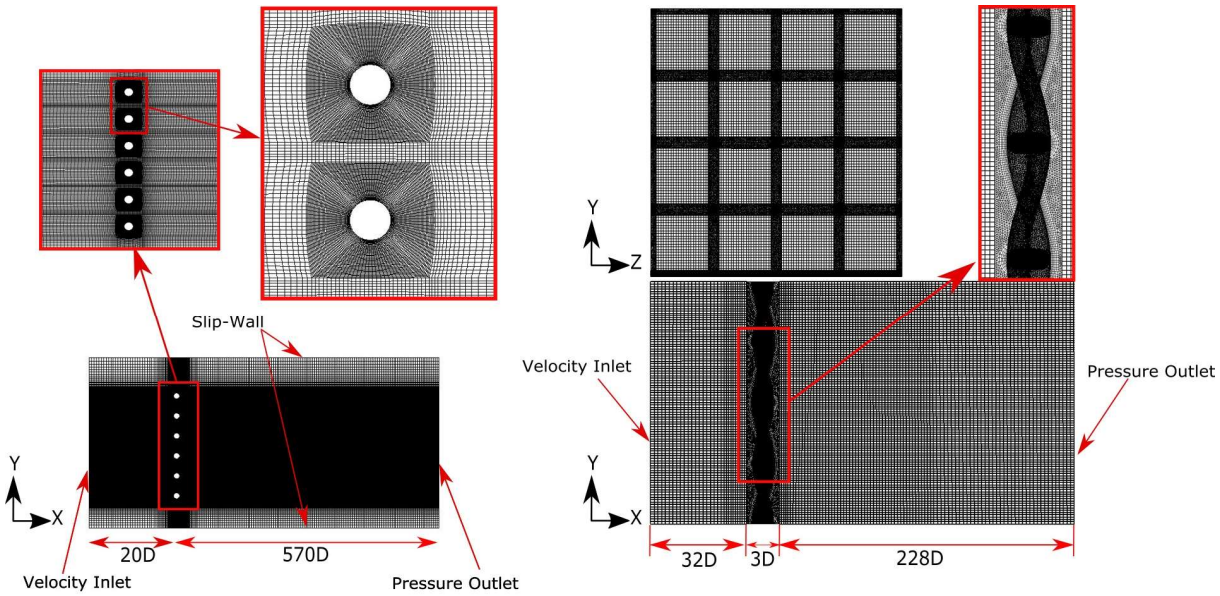

Fig. 3. Numerical Grid showing Boundary conditions

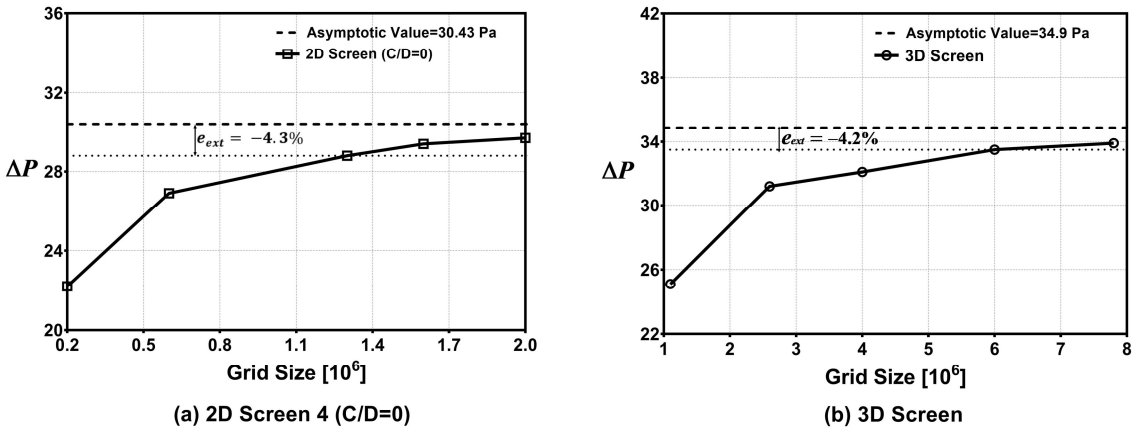

Fig. 4. Grid Independence study of screen 4 showing RE asymptotic values and errors

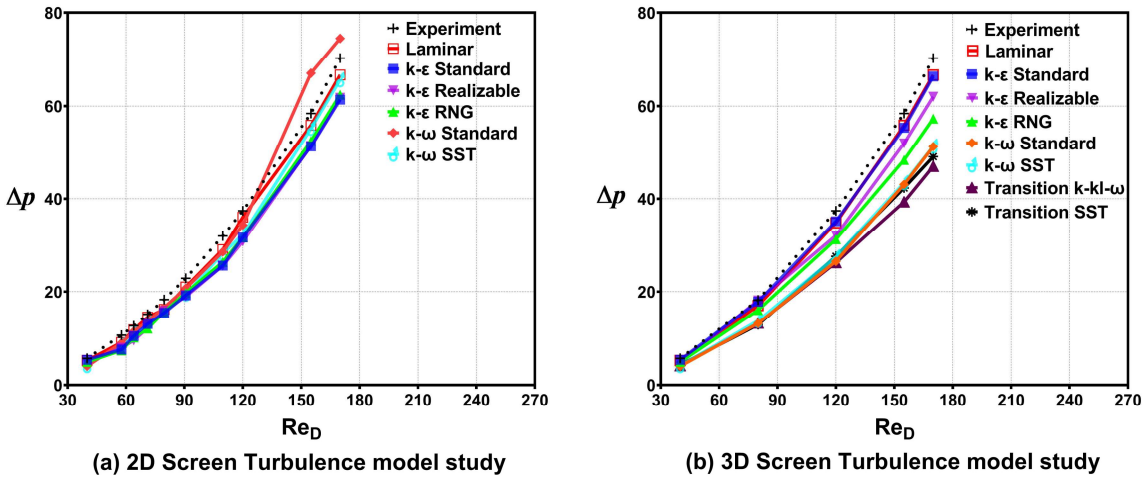

Fig. 5. Screen Turbulence model selection study; Δp [Pa] vs Re_D

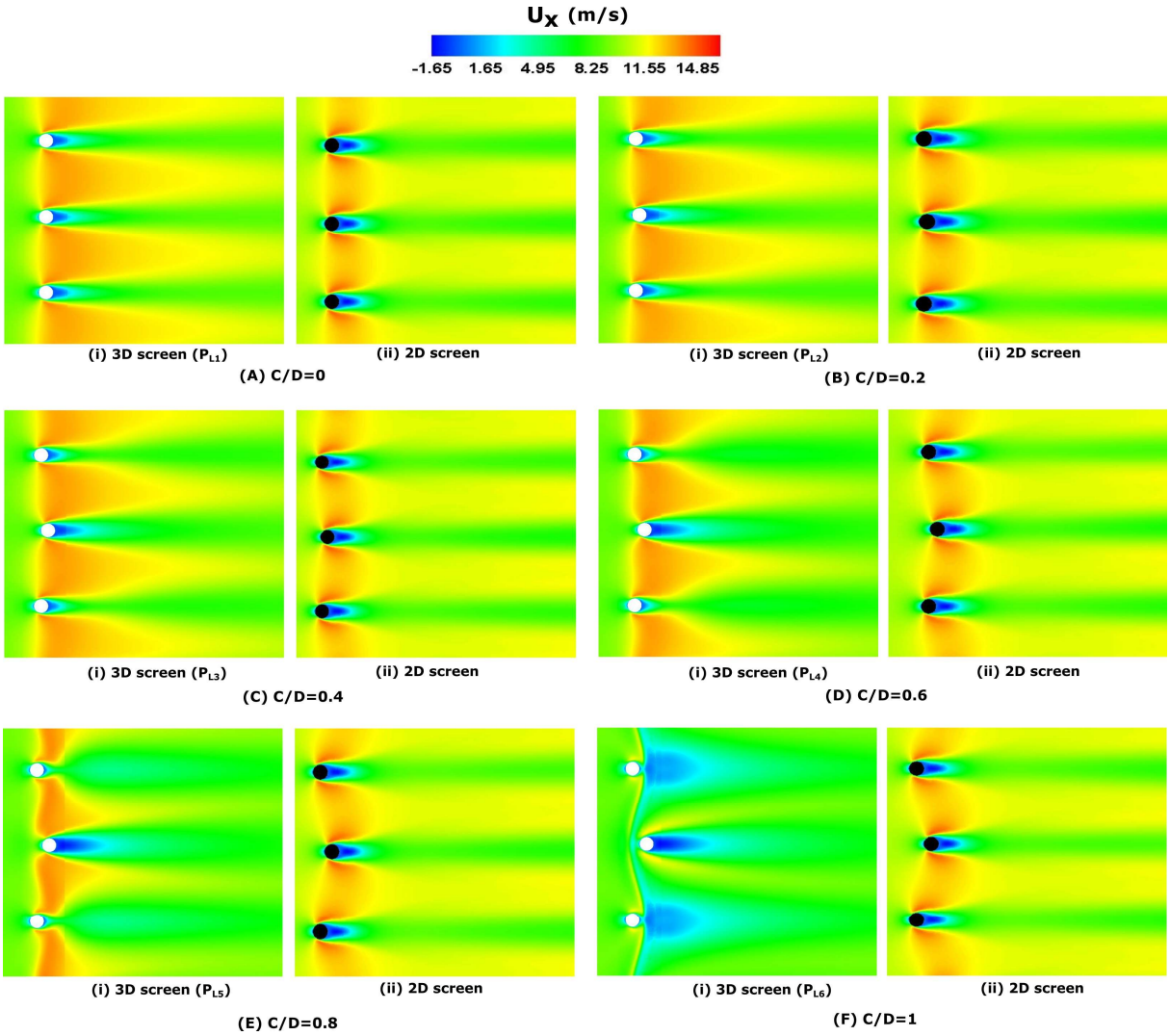

Fig. 6. 3D vs 2D screen (screen sample 4) velocity field comparison. $Re = 120$, $D = 0.19mm$, $P/D = 5.56$ and $0 \leq \frac{C}{D} \leq 1$

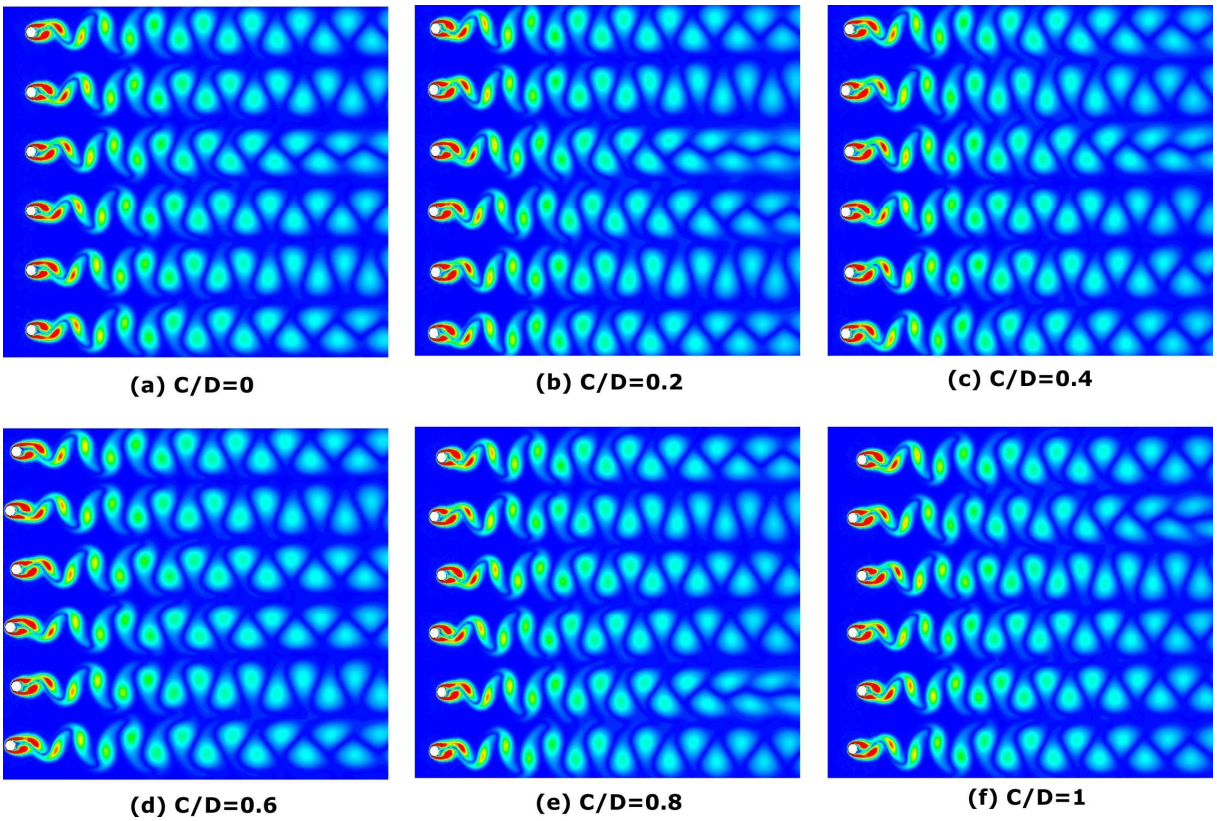

Fig. 7. Instantaneous vorticity magnitude of wake flow past 2D screen 4 configuration $Re = 120$, $D = 0.19mm$, $P/D = 5.56$ and $0 \leq \frac{C}{D} \leq 1$

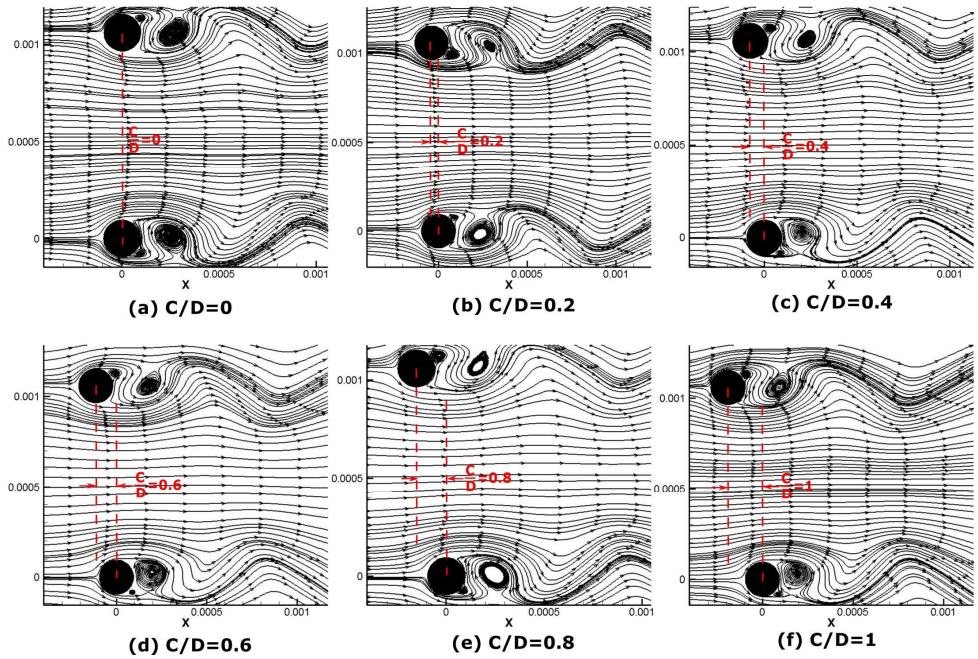

Fig. 8. Unsteady velocity streamlines of wake flow past 2D screen 4; $Re = 120$, $D = 0.1905mm$, $P/D = 5.56$ and $0 \leq \frac{C}{D} \leq 1$

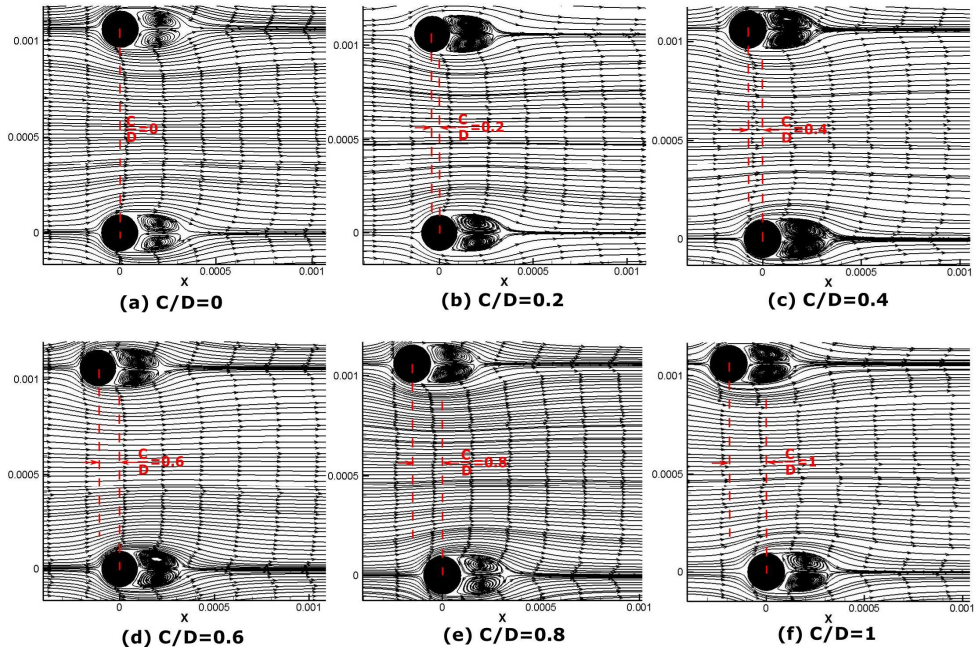

Fig. 9. Mean velocity streamlines of wake flow past 2D screen 4; $Re = 120$, $D = 0.1905mm$, $P/D = 5.56$ and $0 \leq \frac{C}{D} \leq 1$

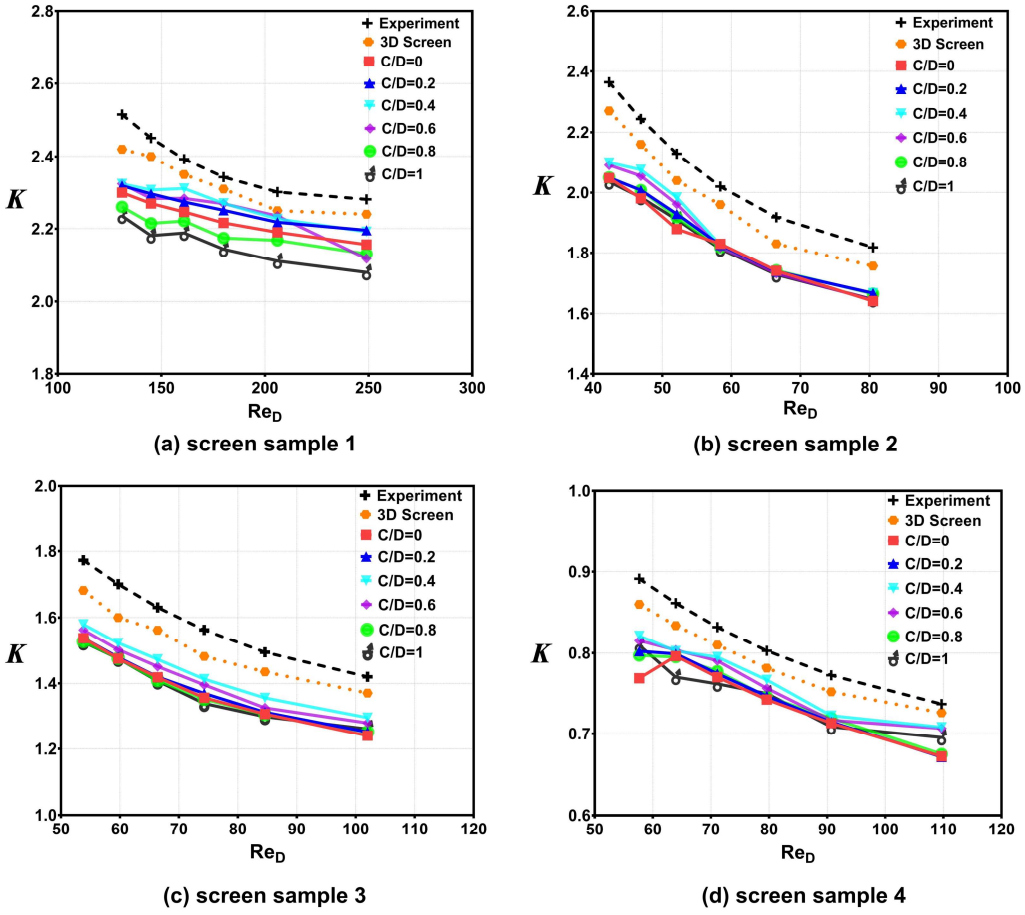

Fig. 10. Comparison of experiment to both 2D and 3D CFD; K vs Re_D

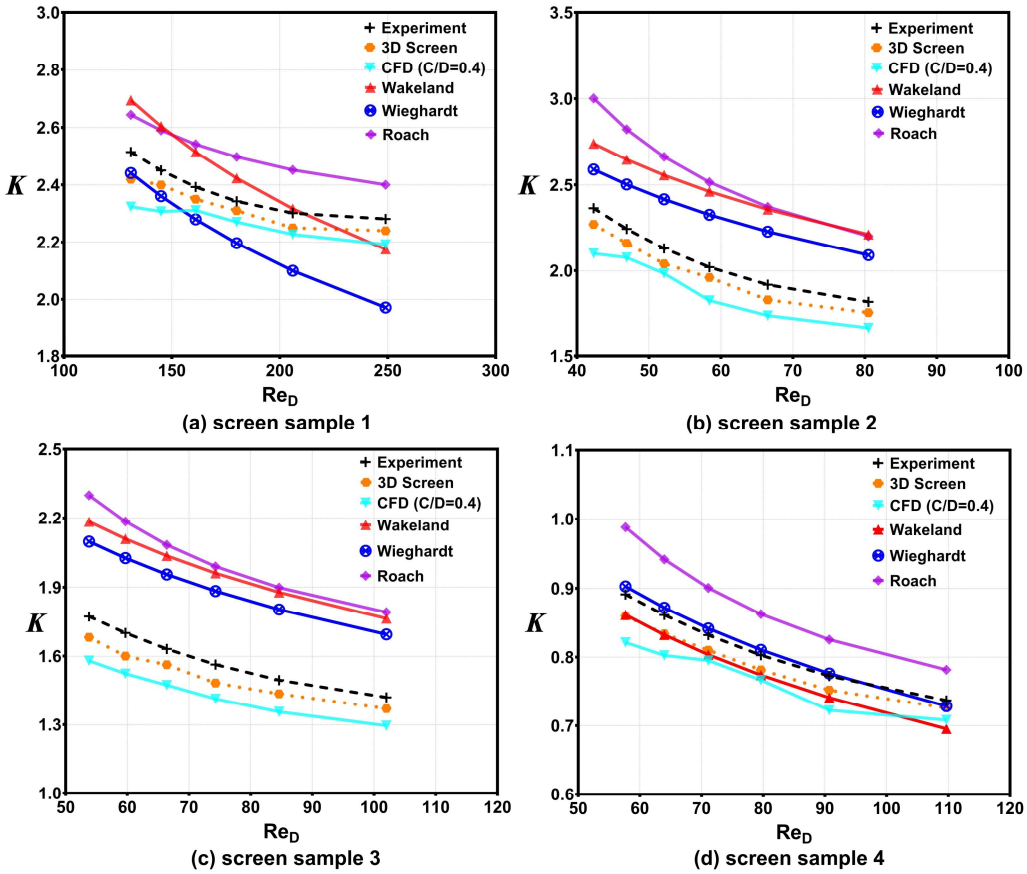

Fig. 11. Flow loss coefficients of numerical analysis: 3D and 2D (C/D=0.4) and experimental results compared with previously published correlations.

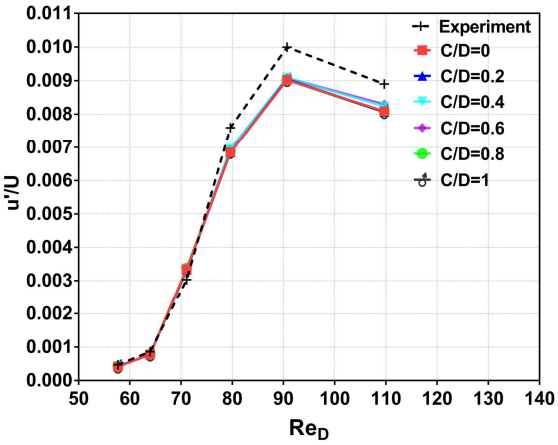

Fig. 12. Axial turbulence intensity 556D downstream screen 4. Experimental values compared to 2D CFD.

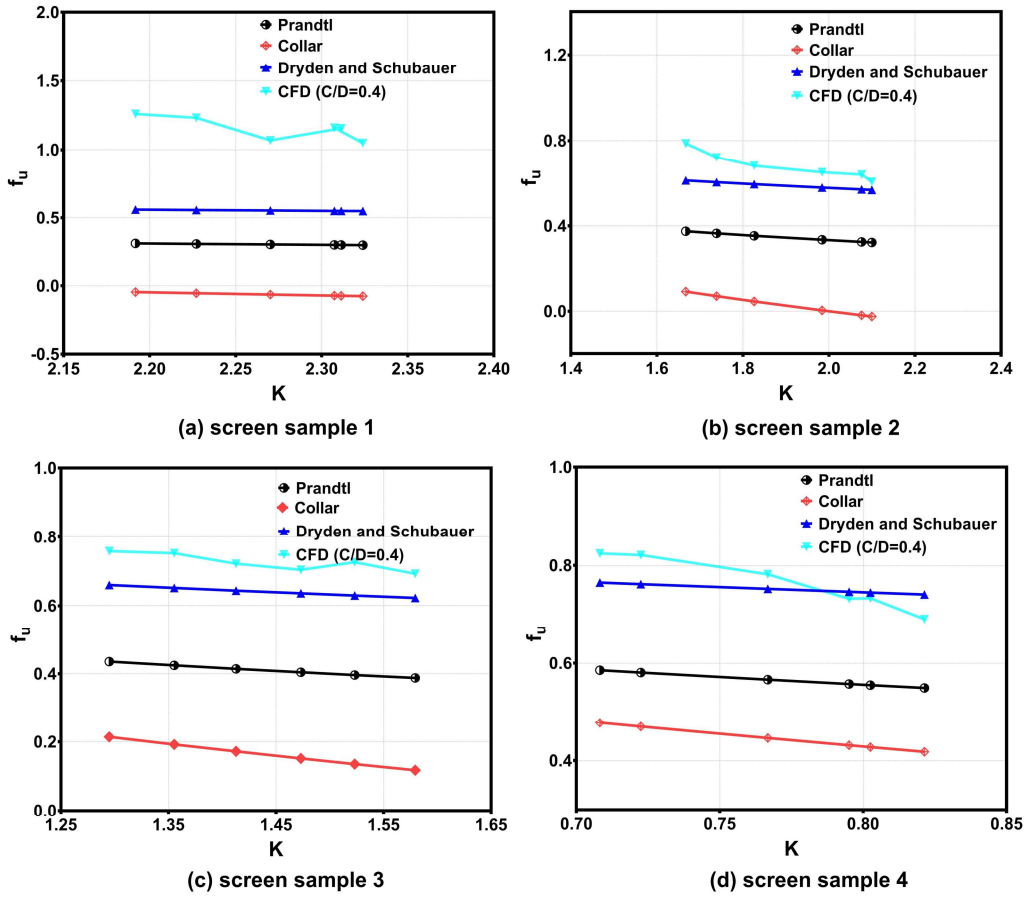

Fig. 13. 2D CFD vs Empirical Models. Turbulence reduction factor f_u against Loss coefficient K.

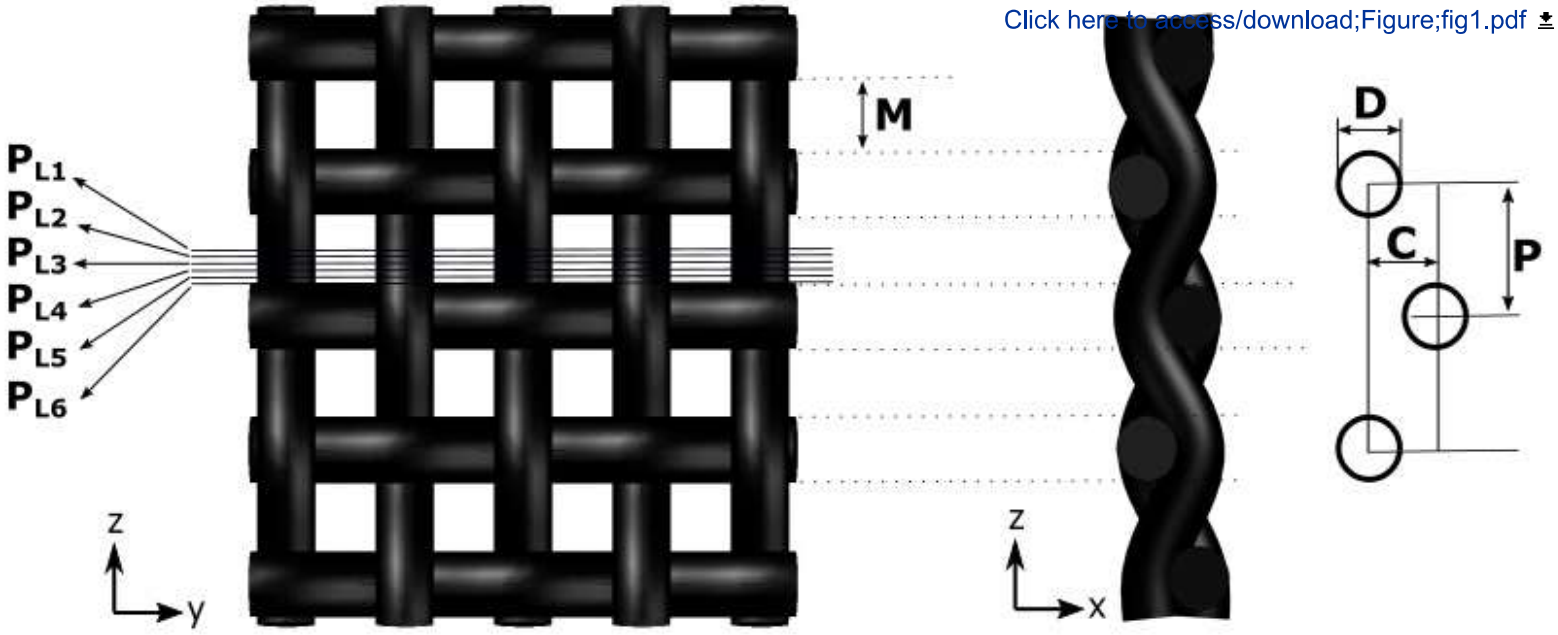

(a) 3D Wire mesh

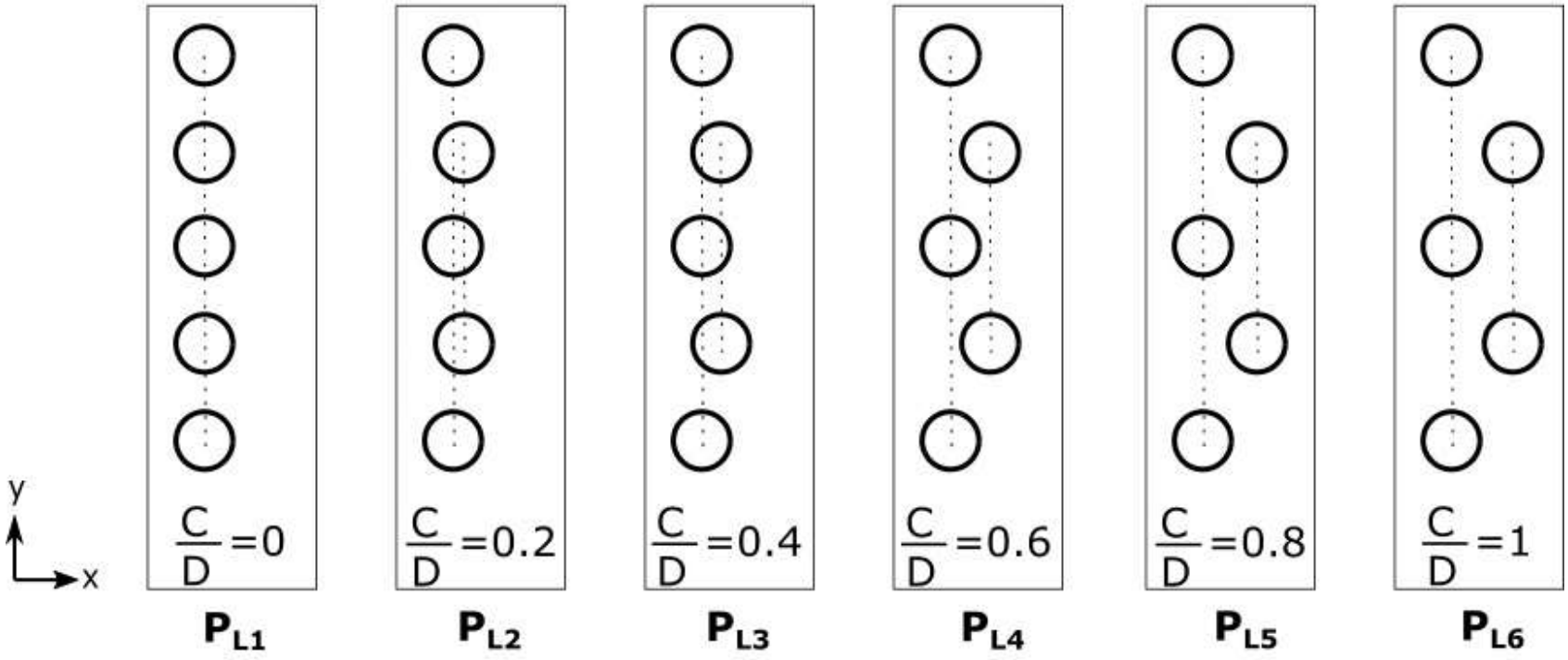

(b) Planes through 3D Wire Mesh

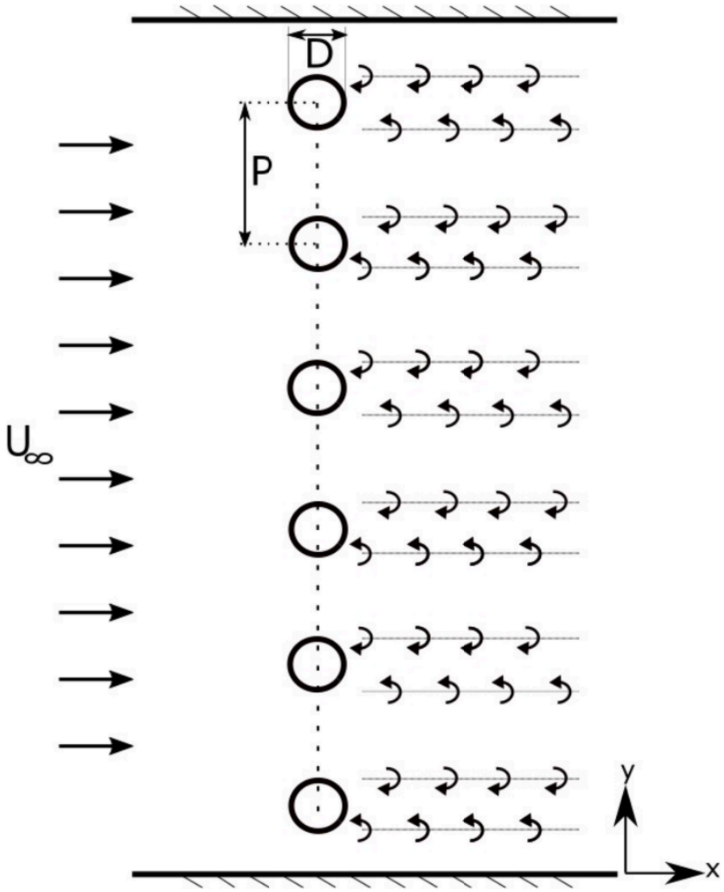

(a) Out of Phase Pattern $2 \leq \frac{P}{D} \leq 6$

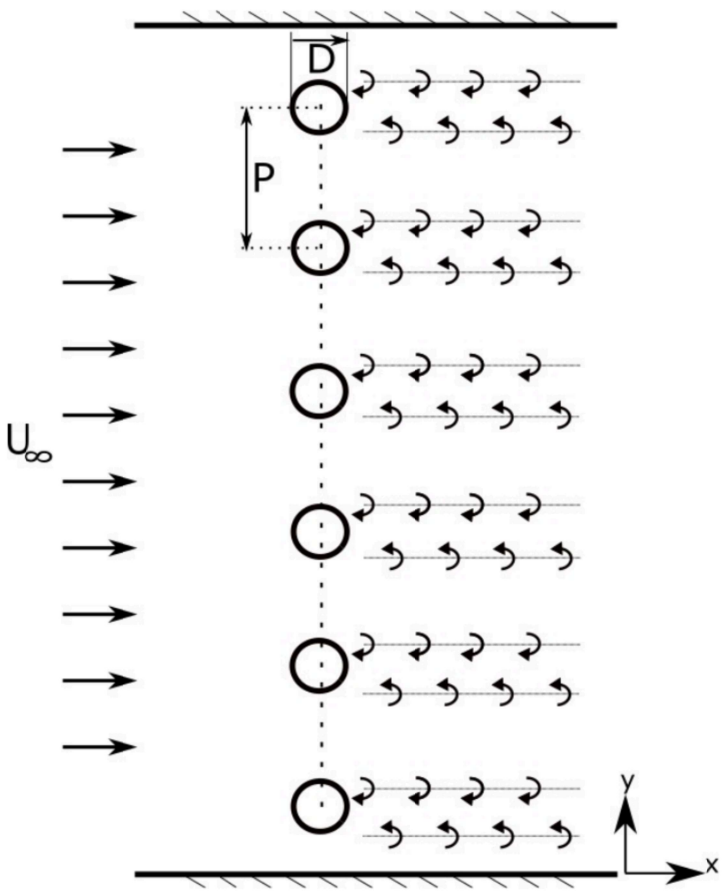

(b) In-Phase Pattern $\frac{P}{D} > 6$

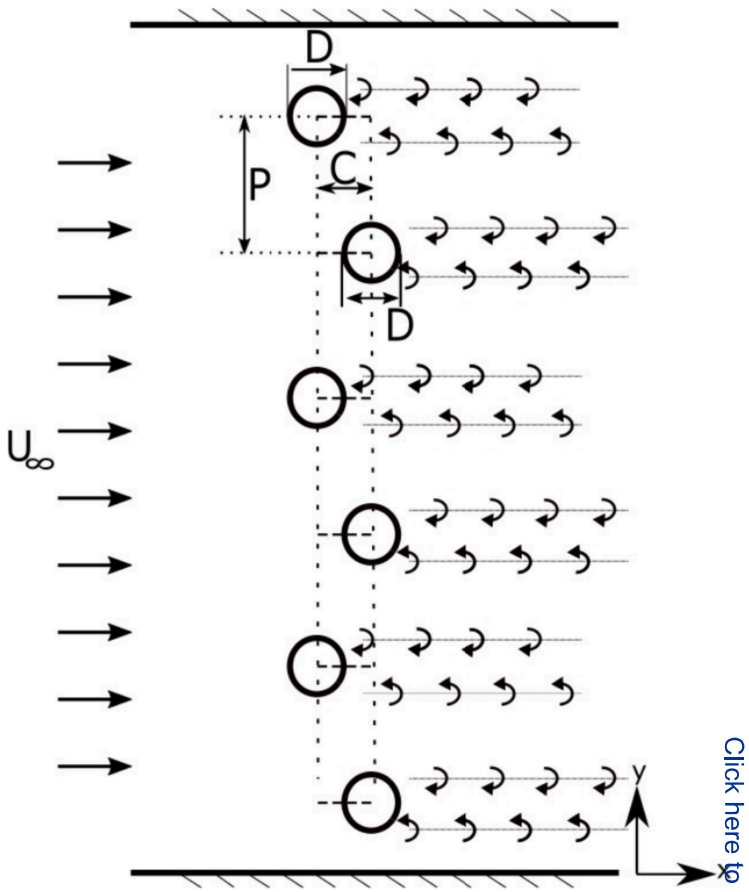

(c) $0 \leq \frac{C}{D} \leq 1$ and $2 \leq \frac{P}{D} \leq 6$

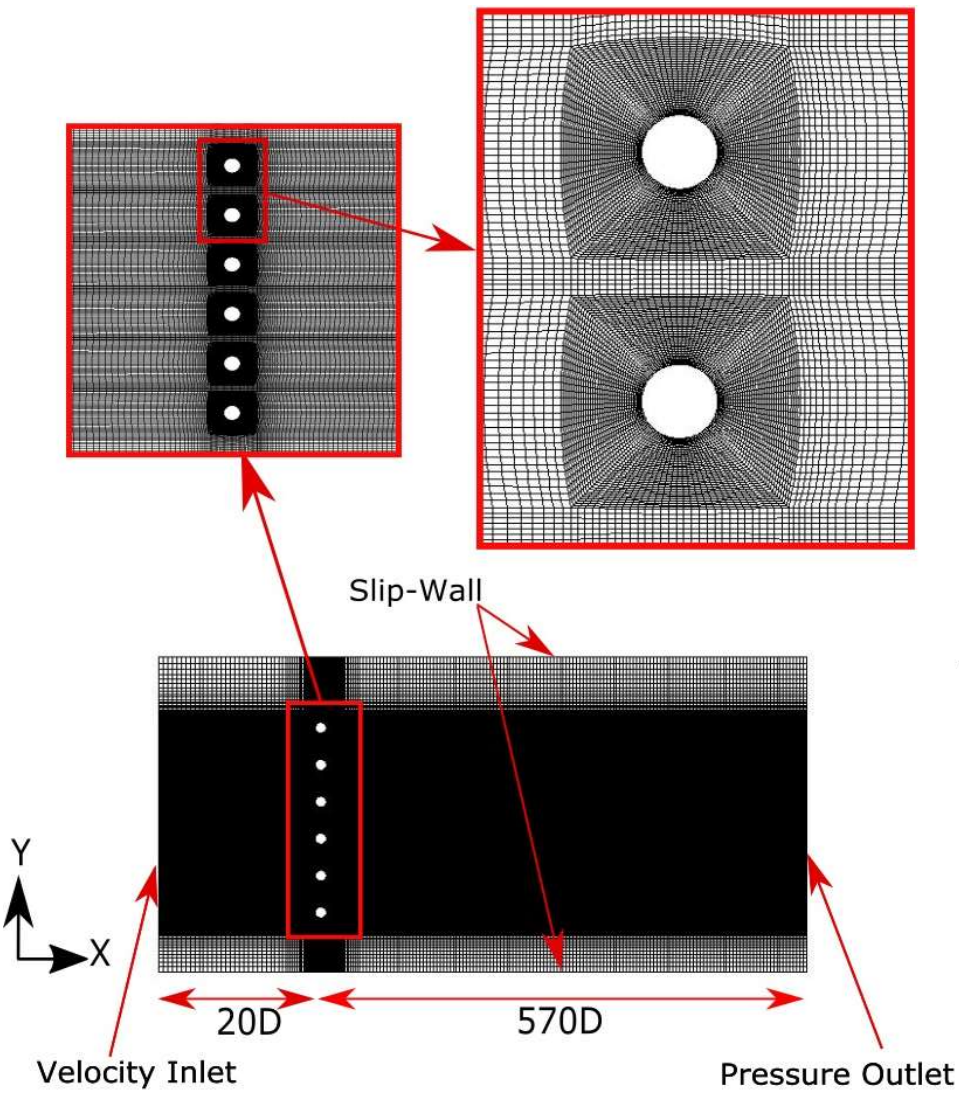

(a) 2D Screen Grid

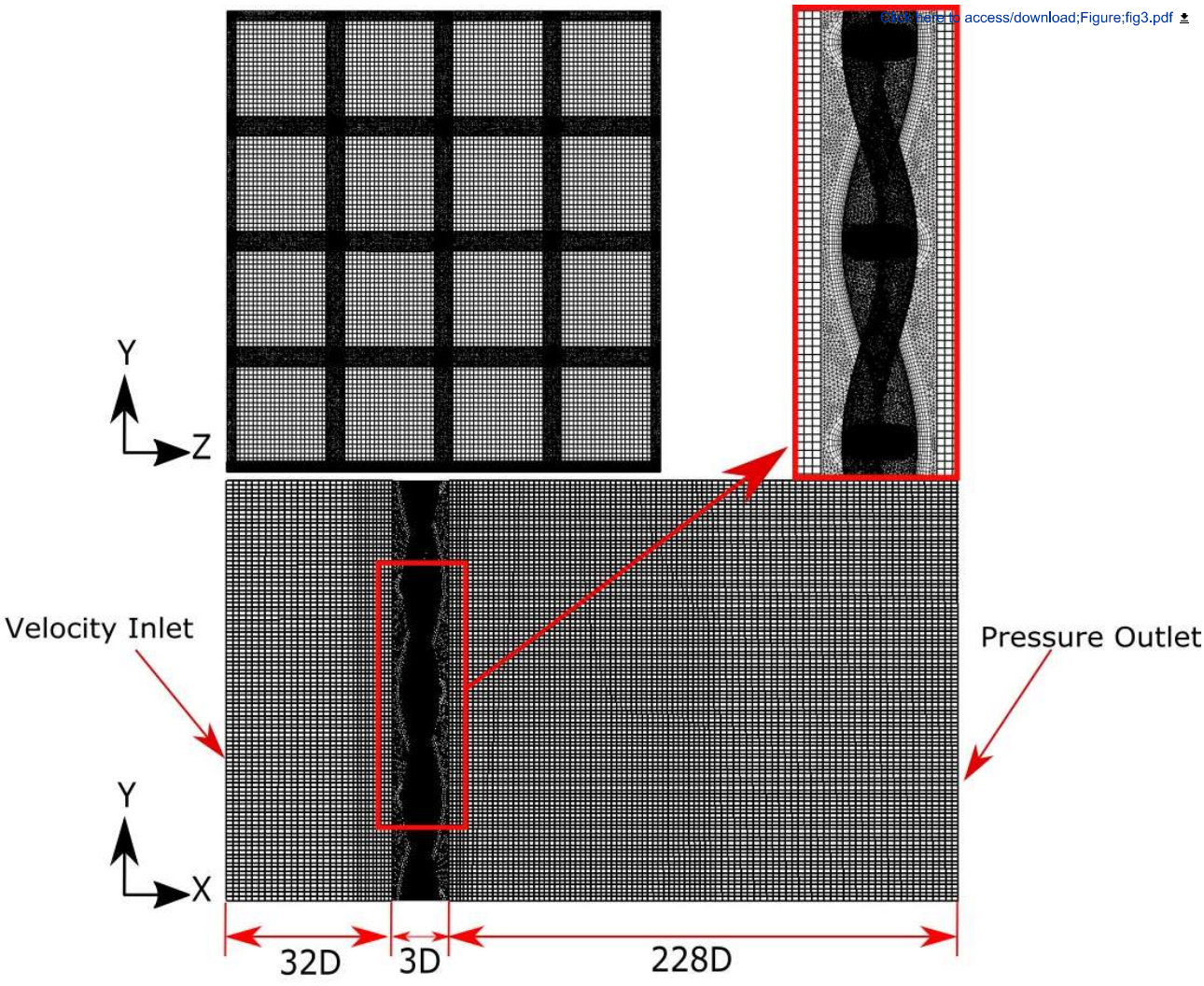

(b) 3D Screen Grid

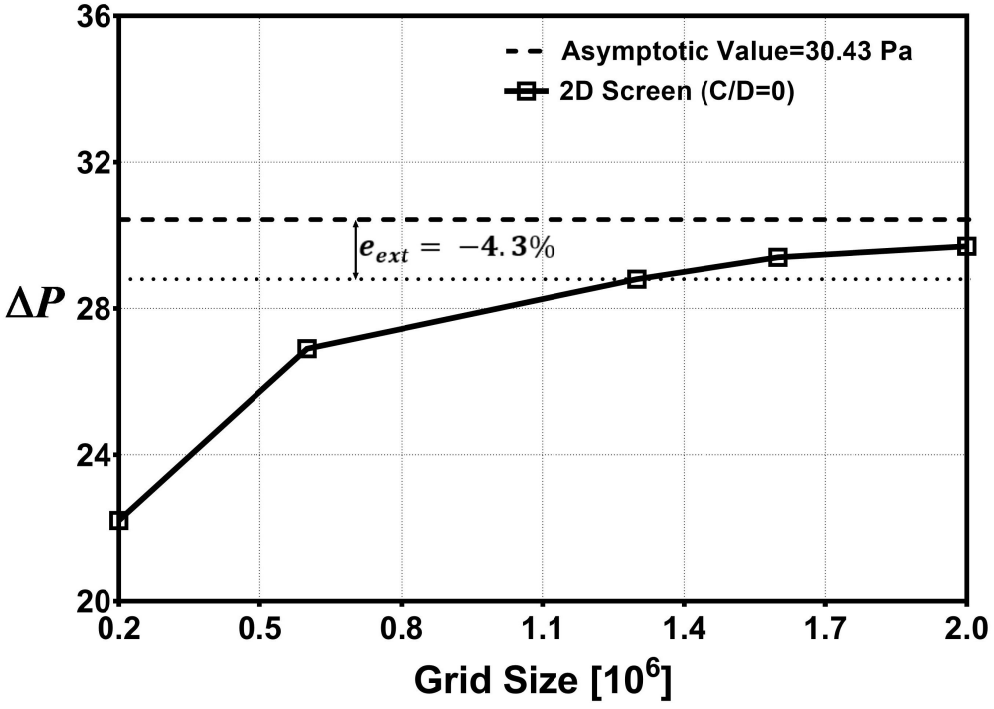

(a) 2D Screen 4 (C/D=0)

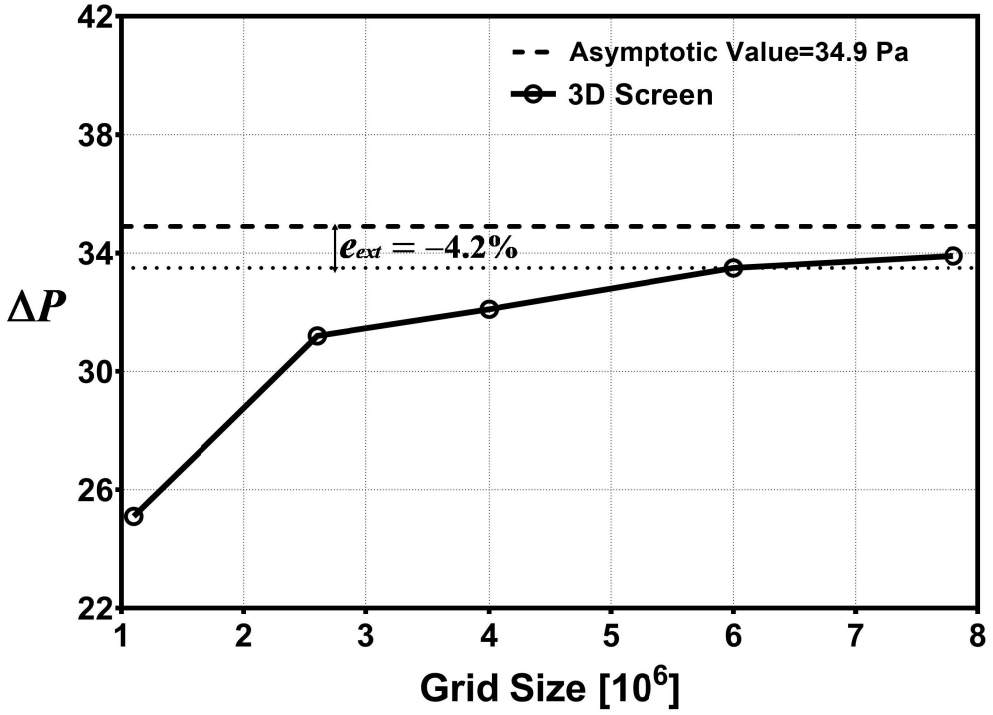

(b) 3D Screen

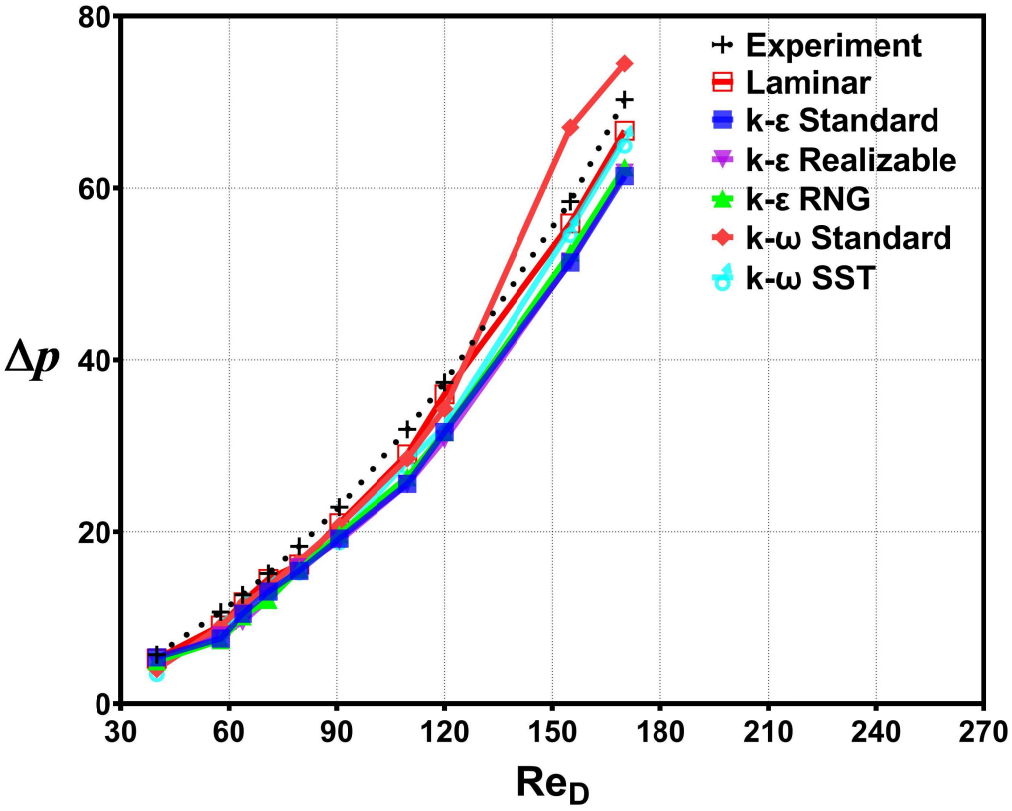

(a) 2D Screen Turbulence model study

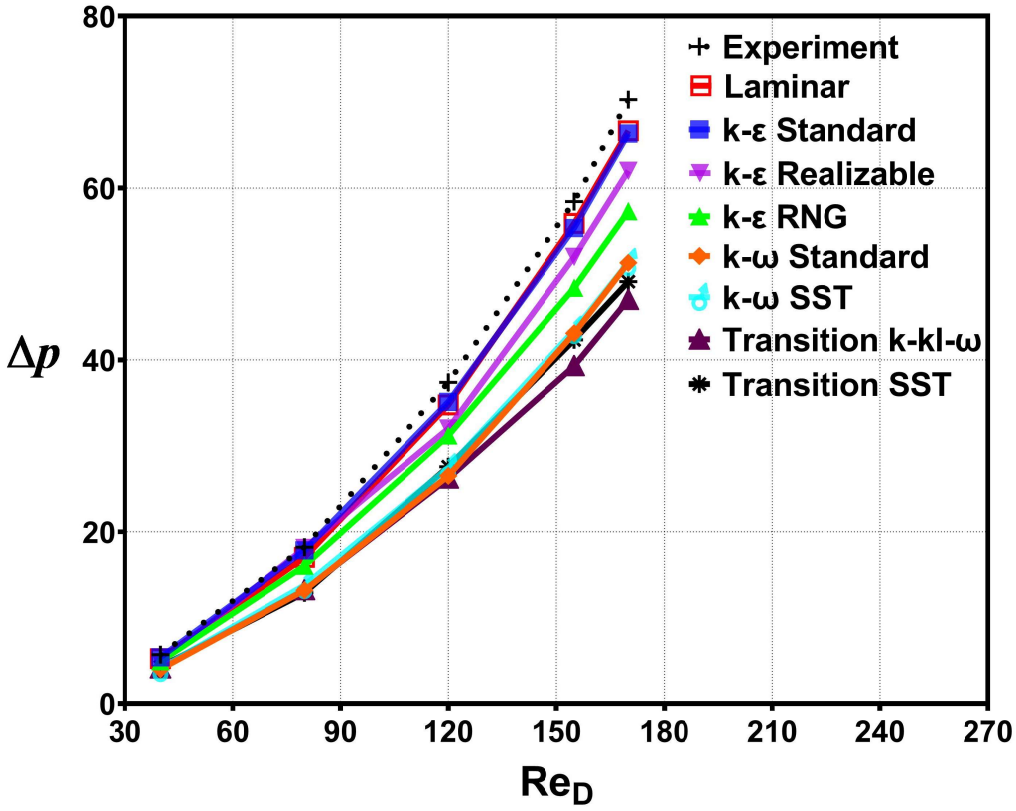

(b) 3D Screen Turbulence model study

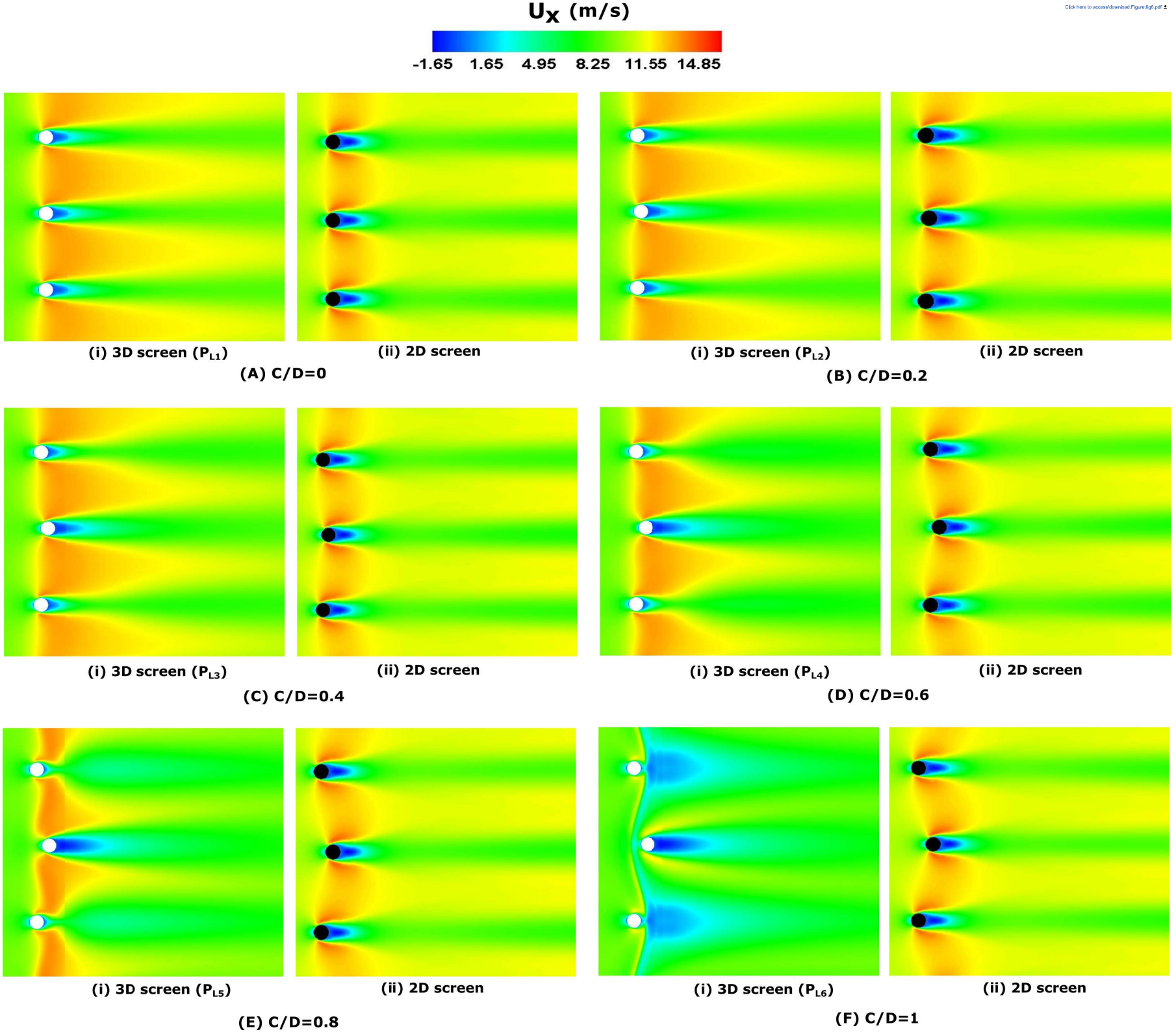

(i) 3D screen (P_{L1}) (ii) 2D screen

(A) C/D=0

(i) 3D screen (P_{L2}) (ii) 2D screen

(B) C/D=0.2

(i) 3D screen (P_{L3}) (ii) 2D screen

(C) C/D=0.4

(i) 3D screen (P_{L4}) (ii) 2D screen

(D) C/D=0.6

(i) 3D screen (P_{L5}) (ii) 2D screen

(E) C/D=0.8

(i) 3D screen (P_{L6}) (ii) 2D screen

(F) C/D=1

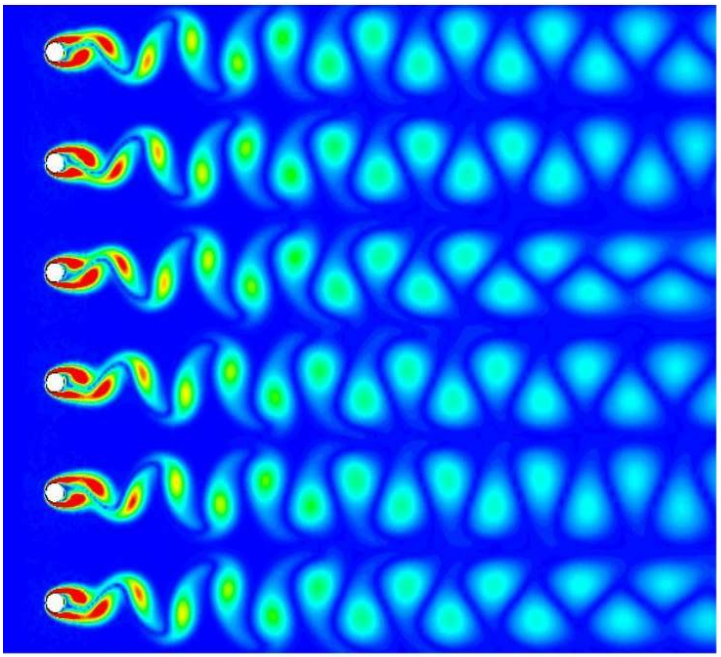

(a) C/D=0

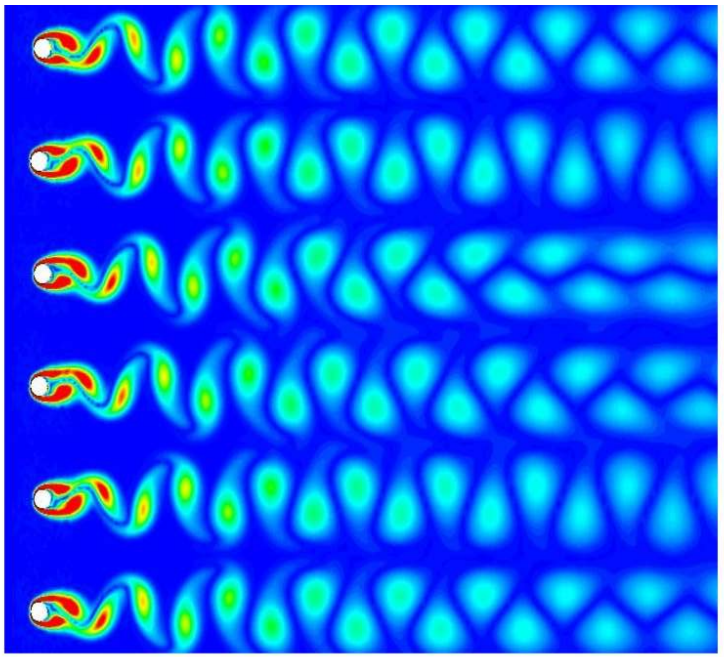

(b) C/D=0.2

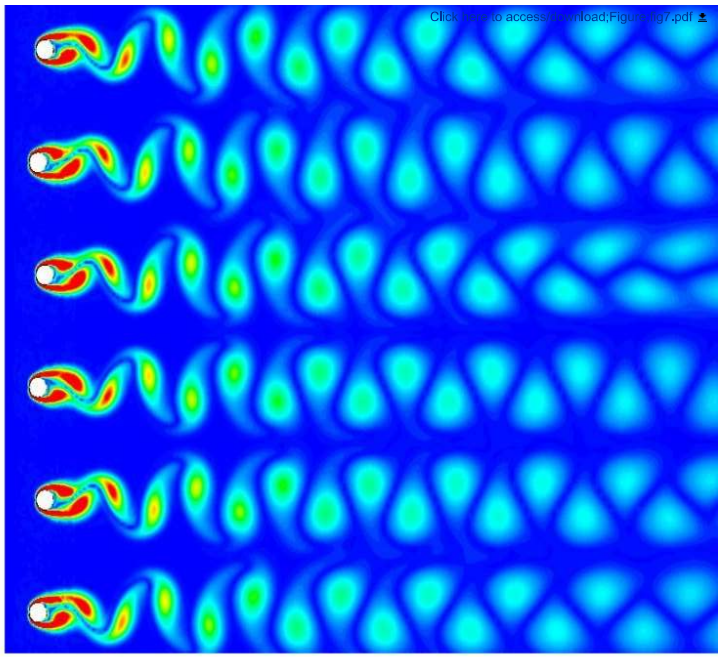

(c) C/D=0.4

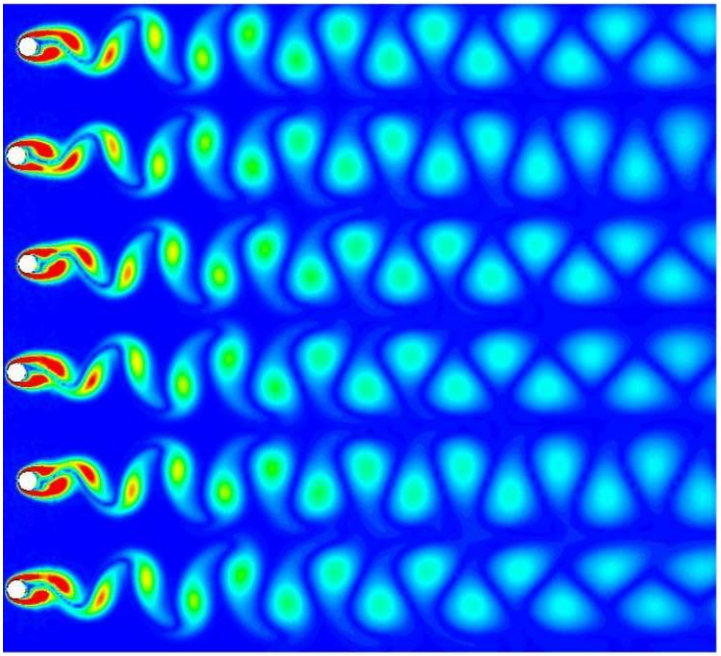

(d) C/D=0.6

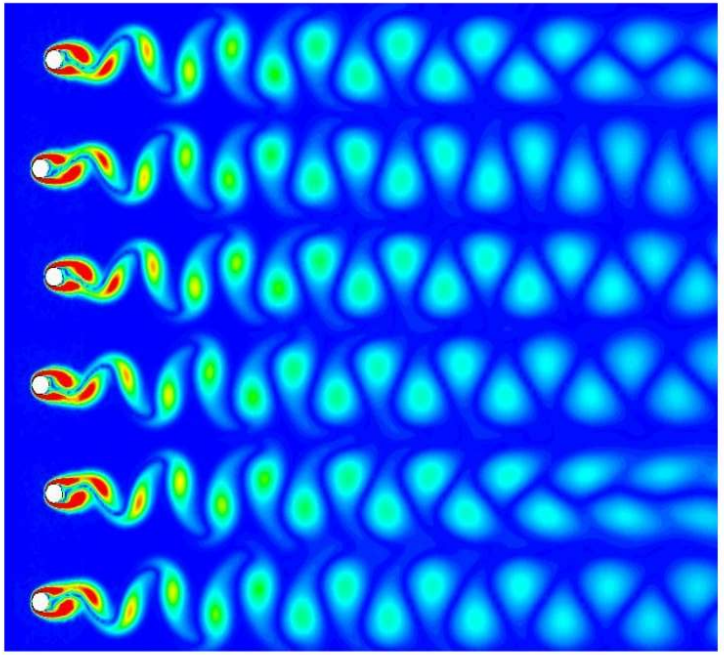

(e) C/D=0.8

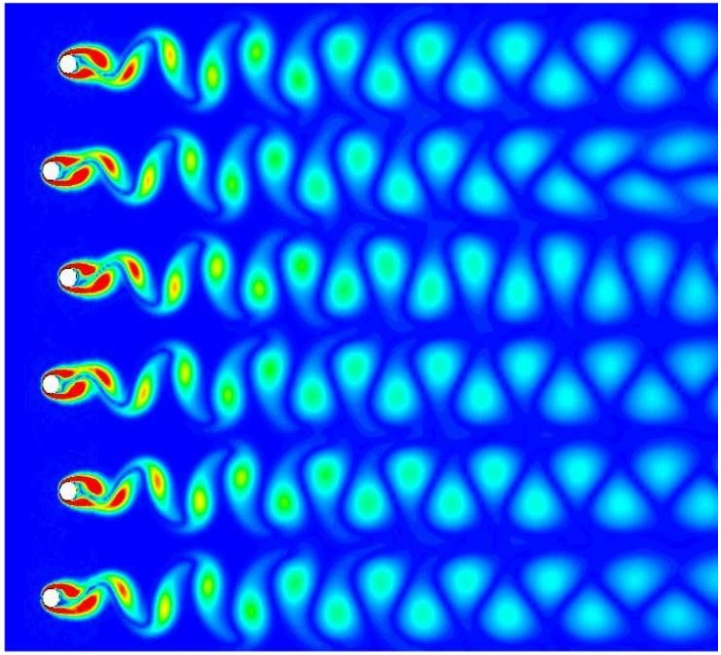

(f) C/D=1

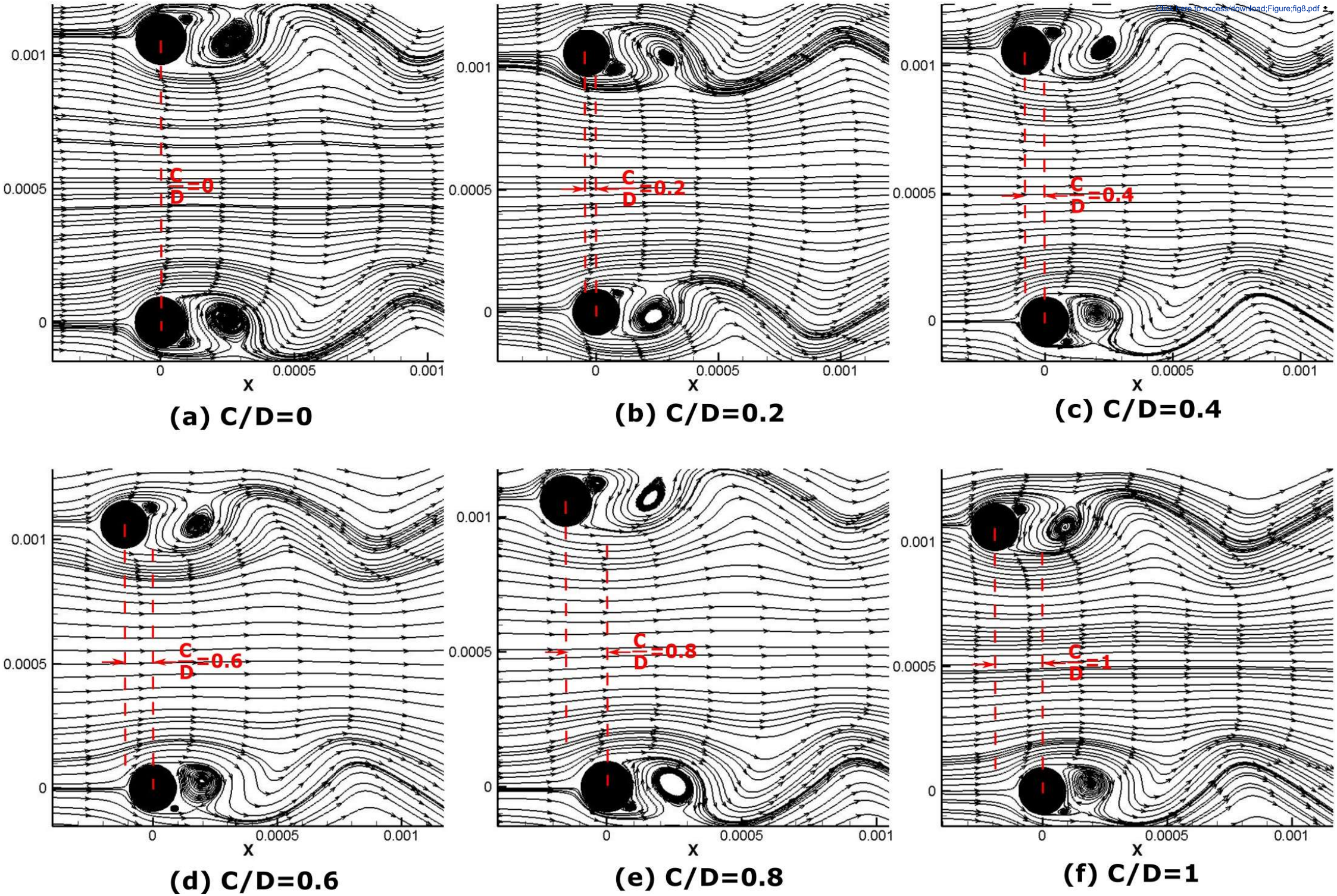

(a) C/D=0

(b) C/D=0.2

(c) C/D=0.4

(d) C/D=0.6

(e) C/D=0.8

(f) C/D=1

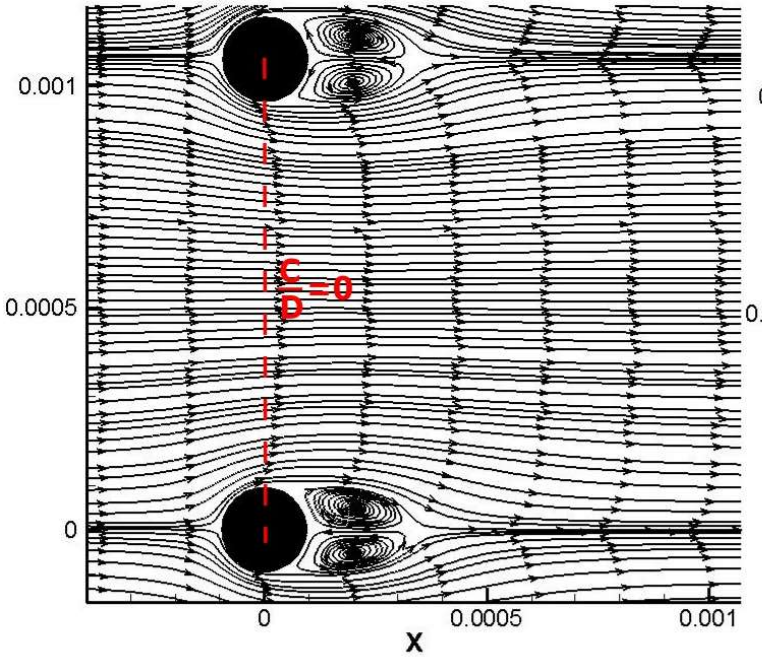

(a) C/D=0

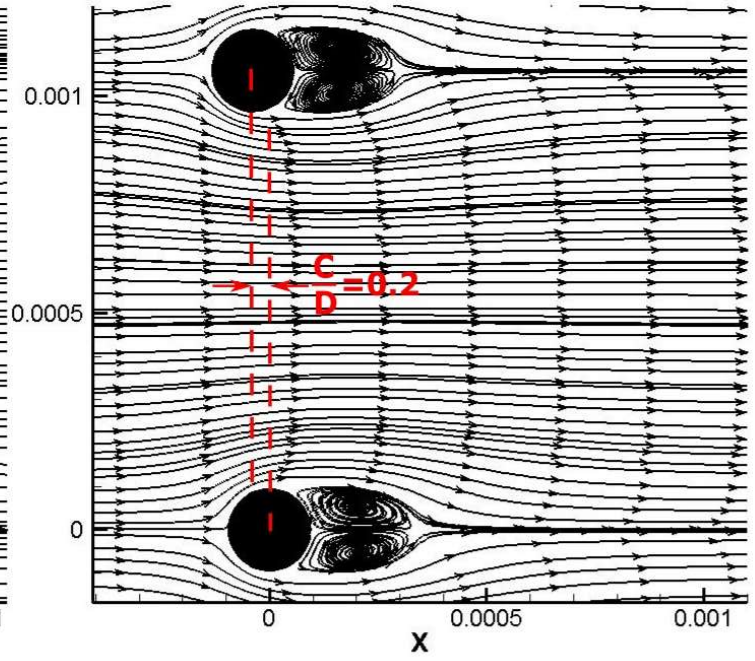

(b) C/D=0.2

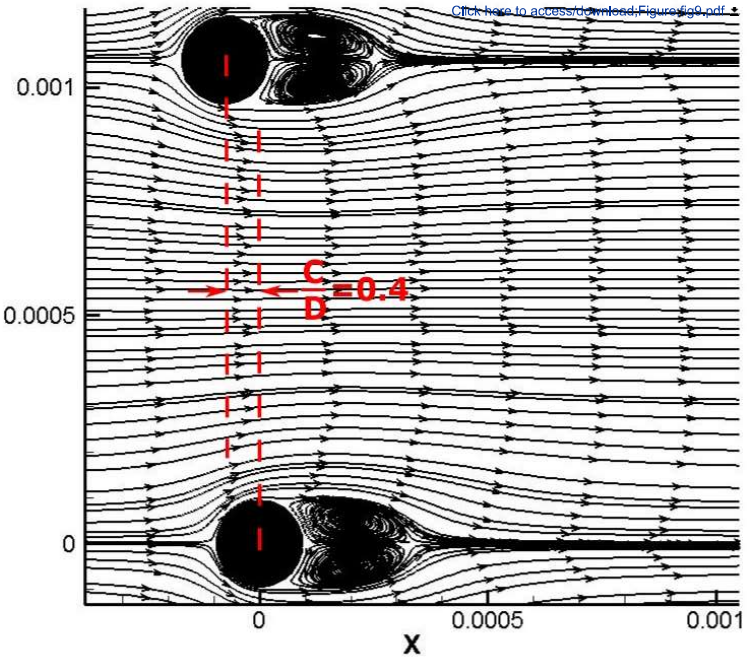

(c) C/D=0.4

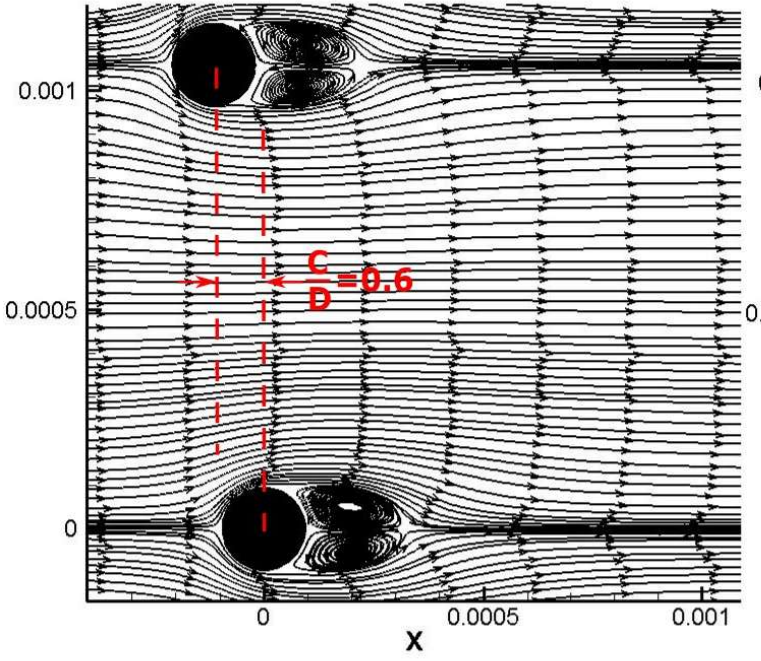

(d) C/D=0.6

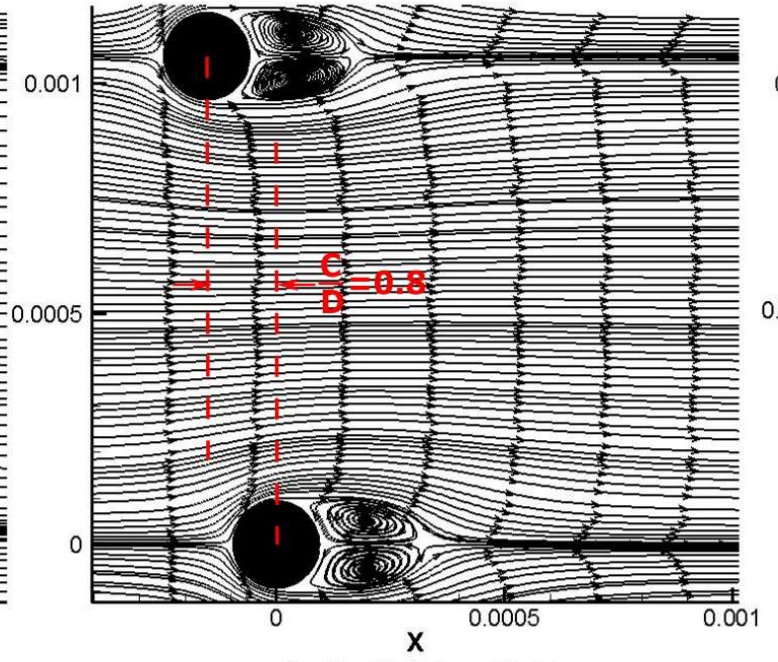

(e) C/D=0.8

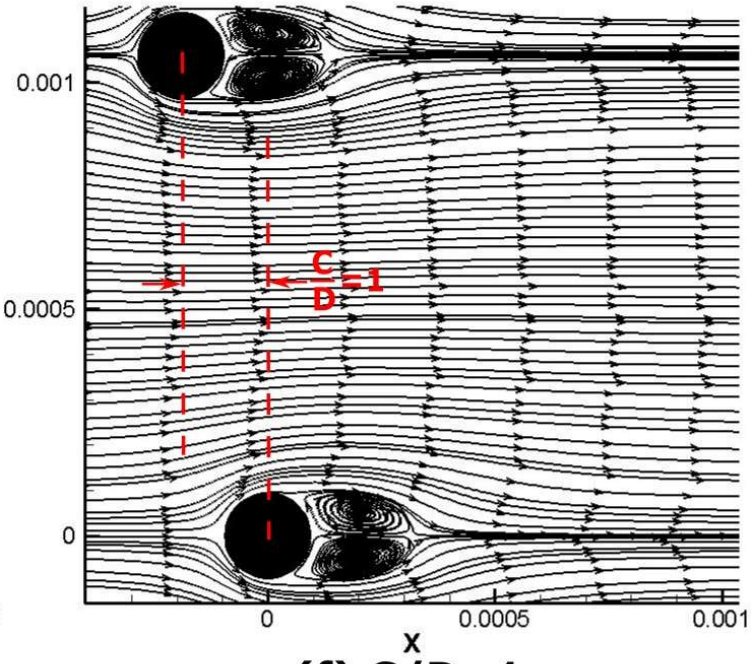

(f) C/D=1

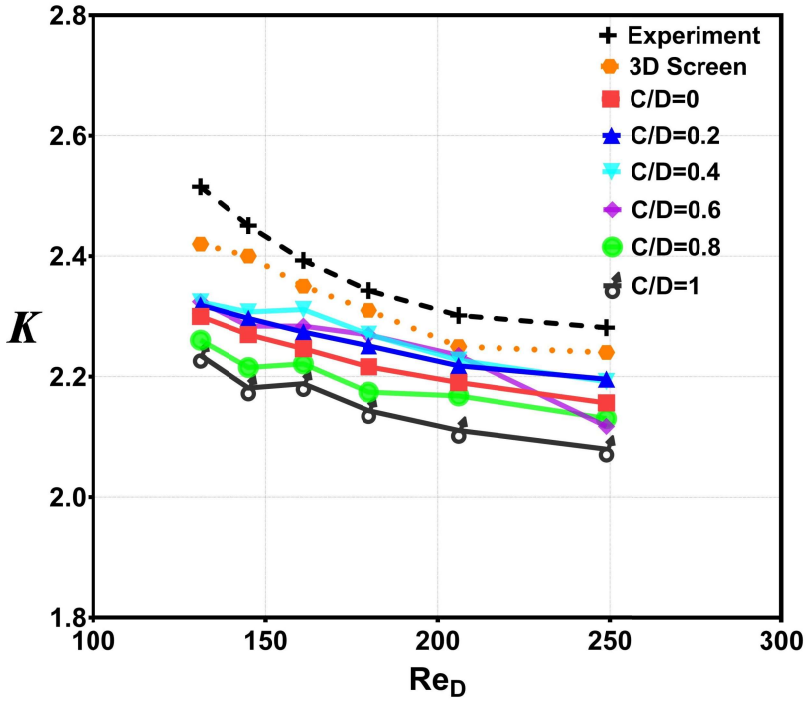

(a) screen sample 1

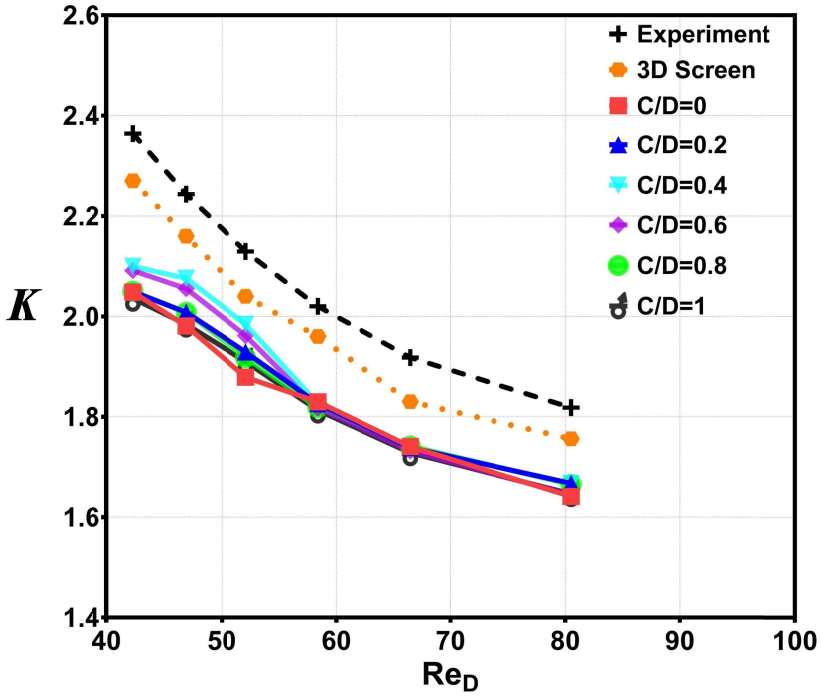

(b) screen sample 2

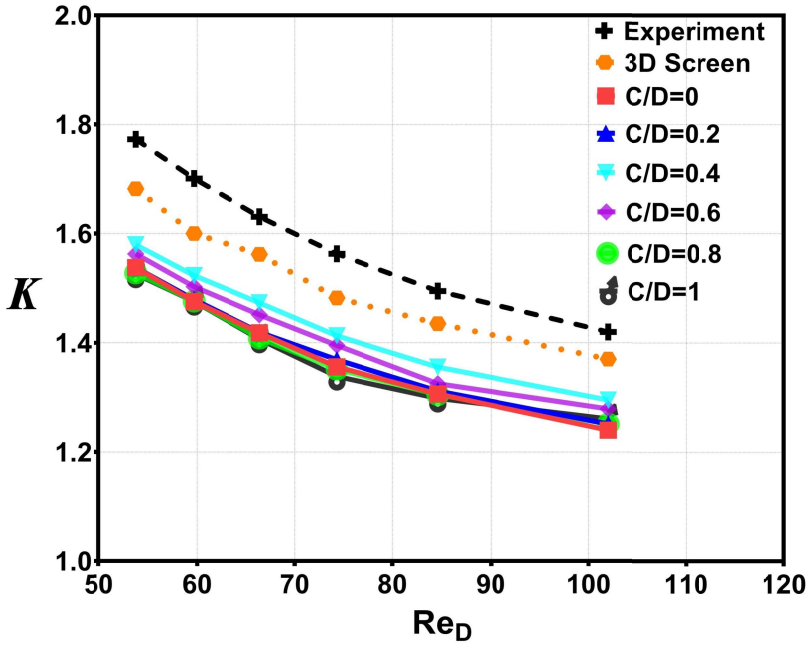

(c) screen sample 3

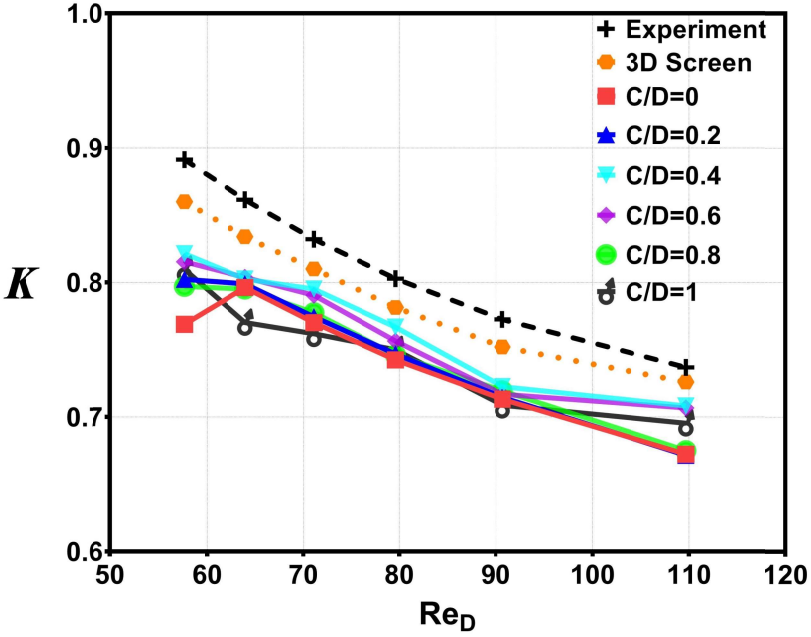

(d) screen sample 4

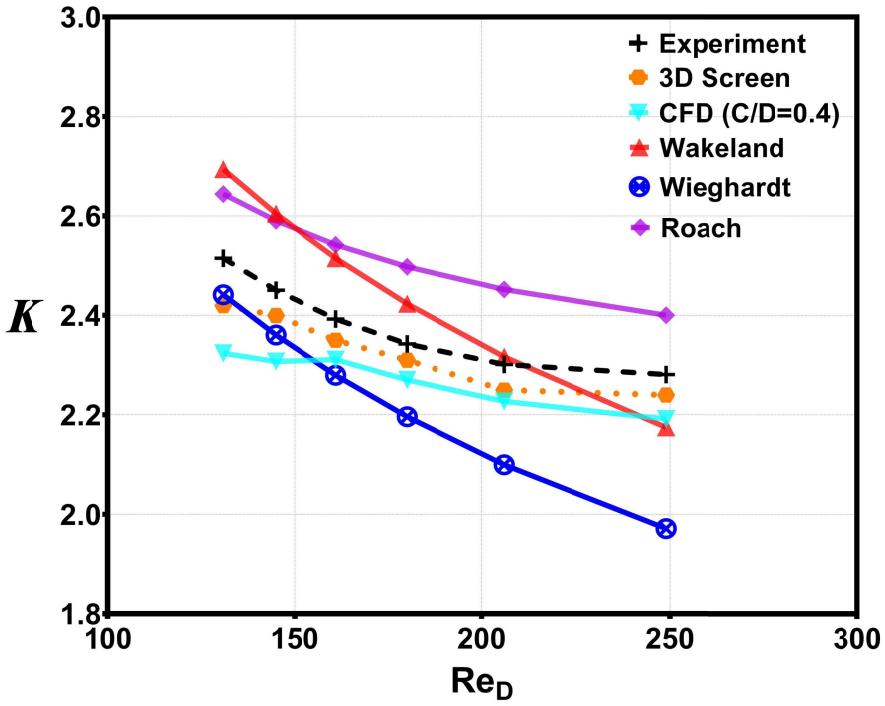

(a) screen sample 1

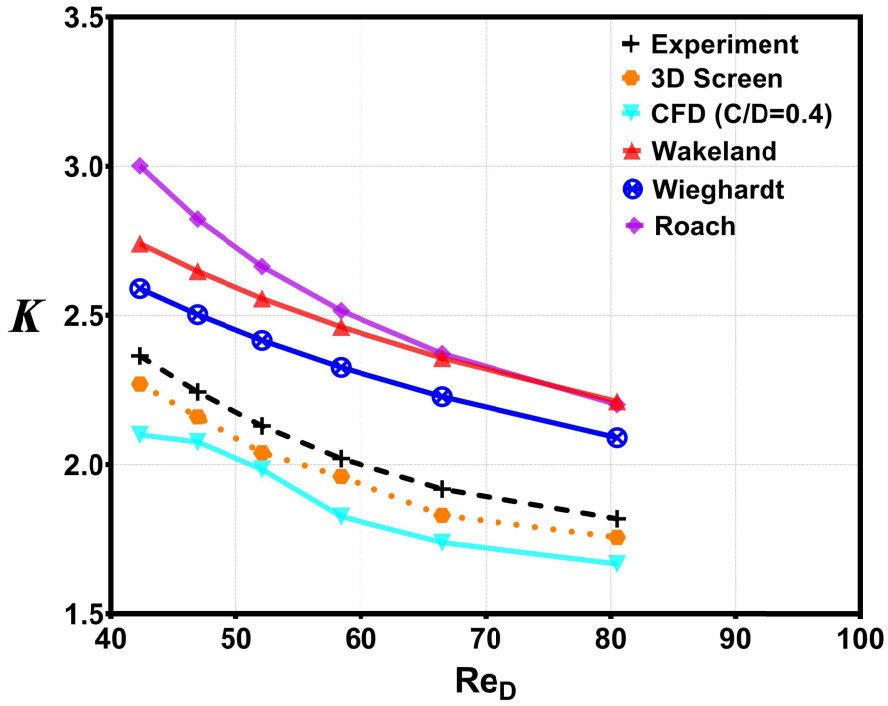

(b) screen sample 2

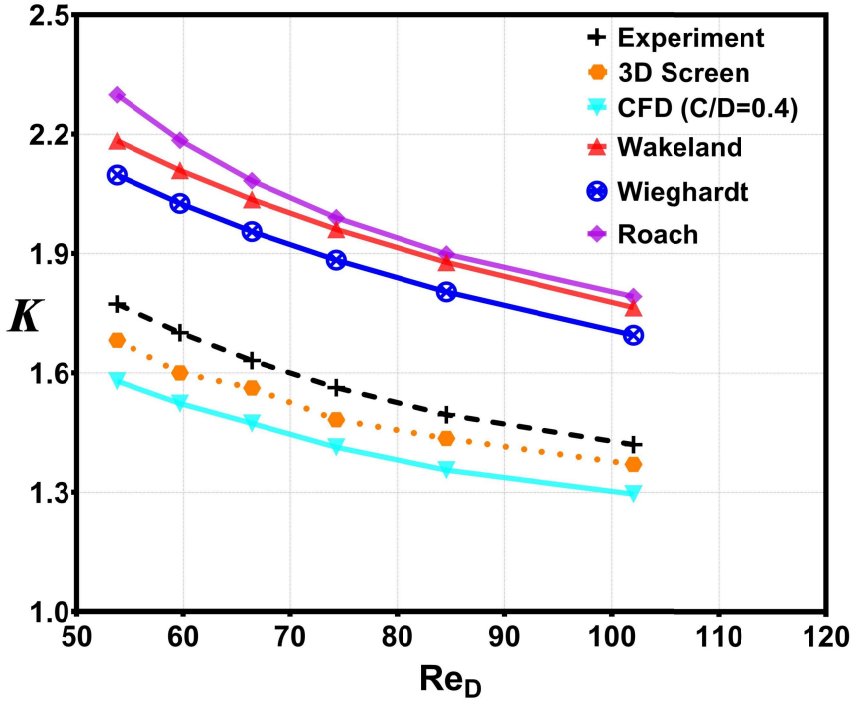

(c) screen sample 3

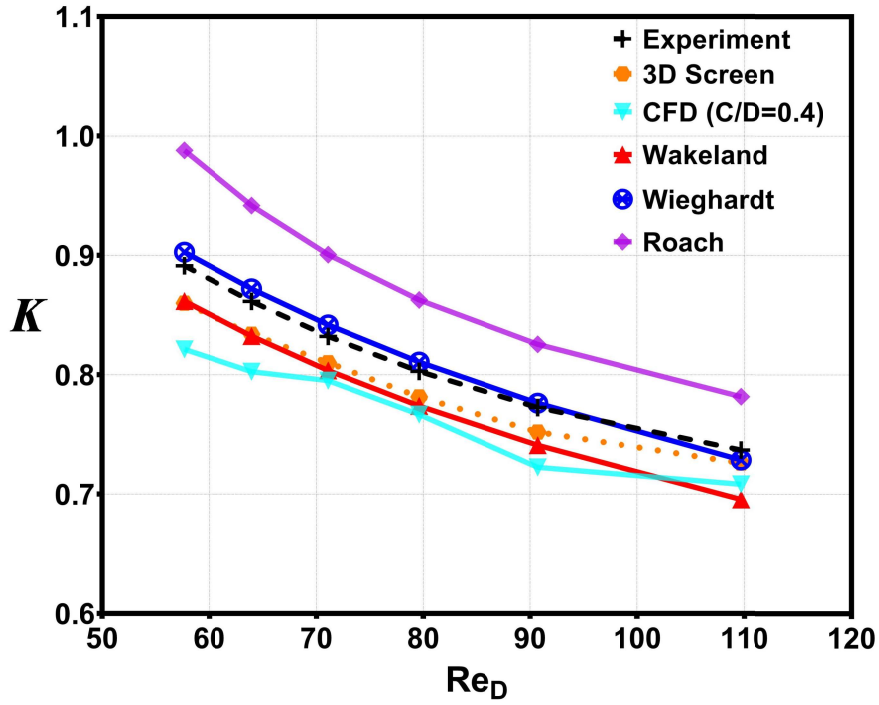

(d) screen sample 4

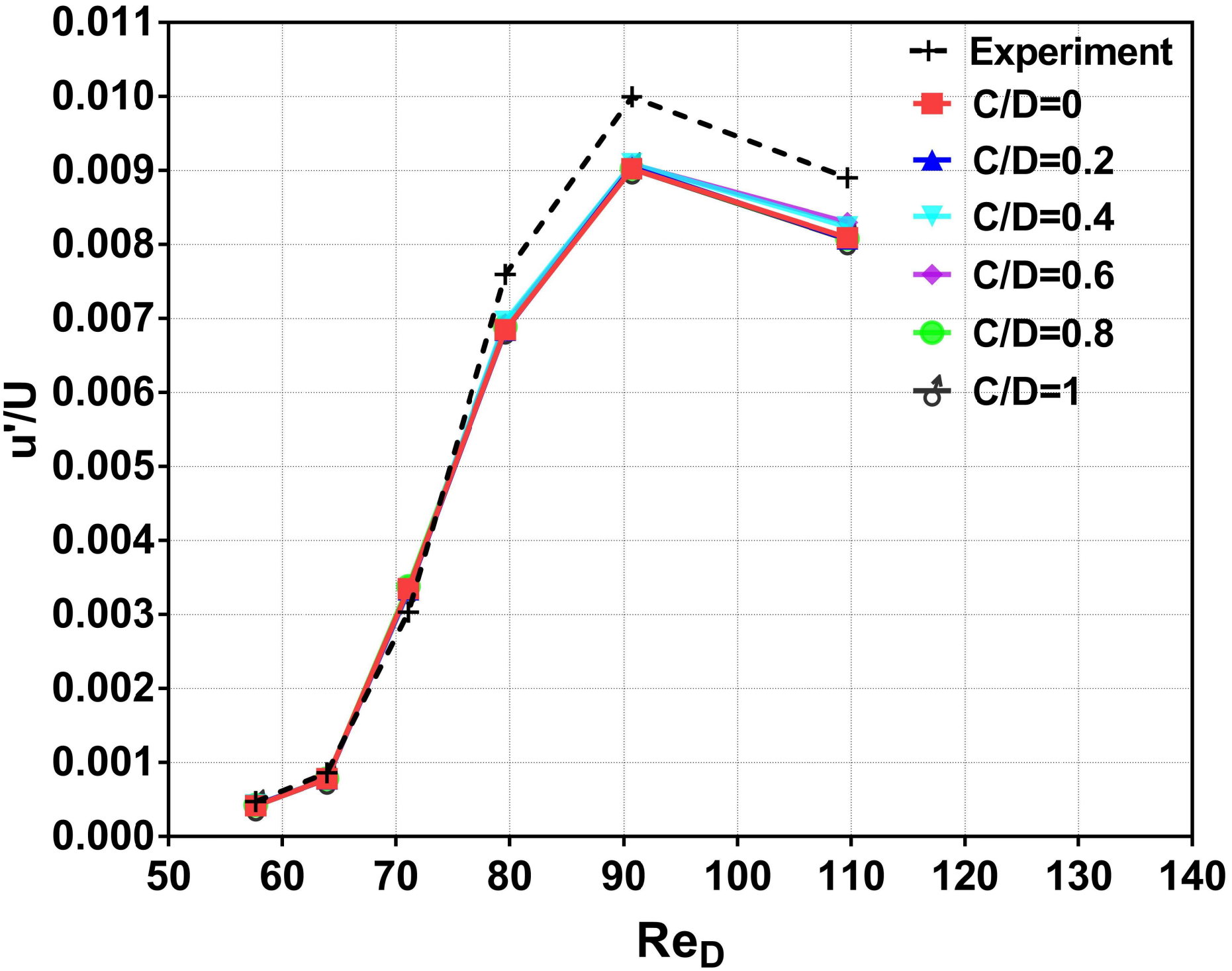

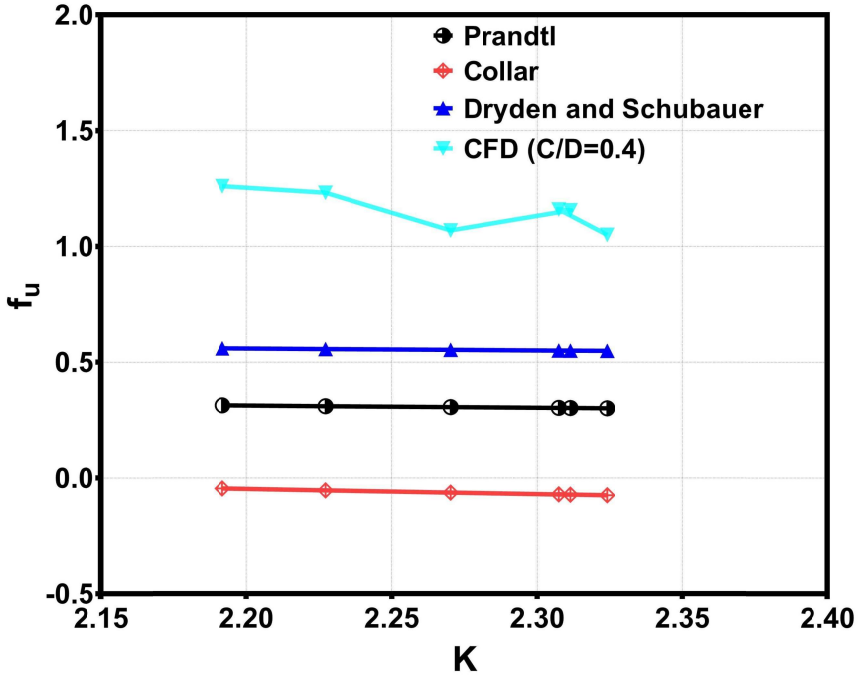

(a) screen sample 1

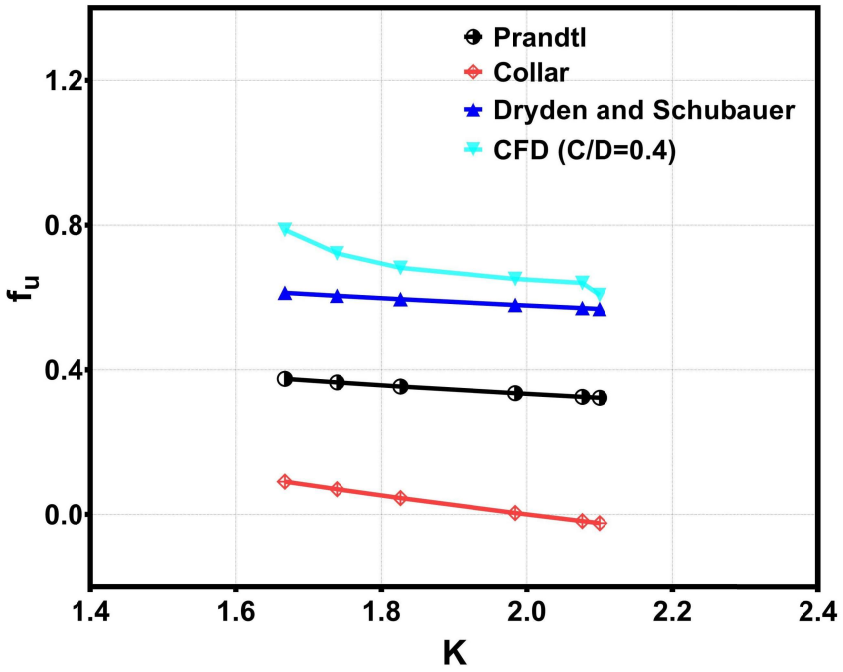

(b) screen sample 2

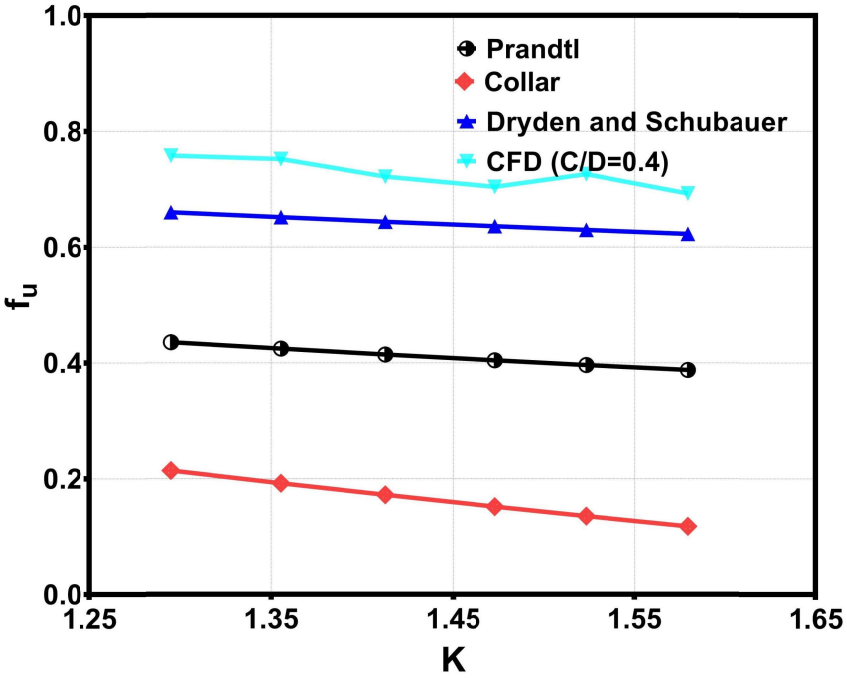

(c) screen sample 3

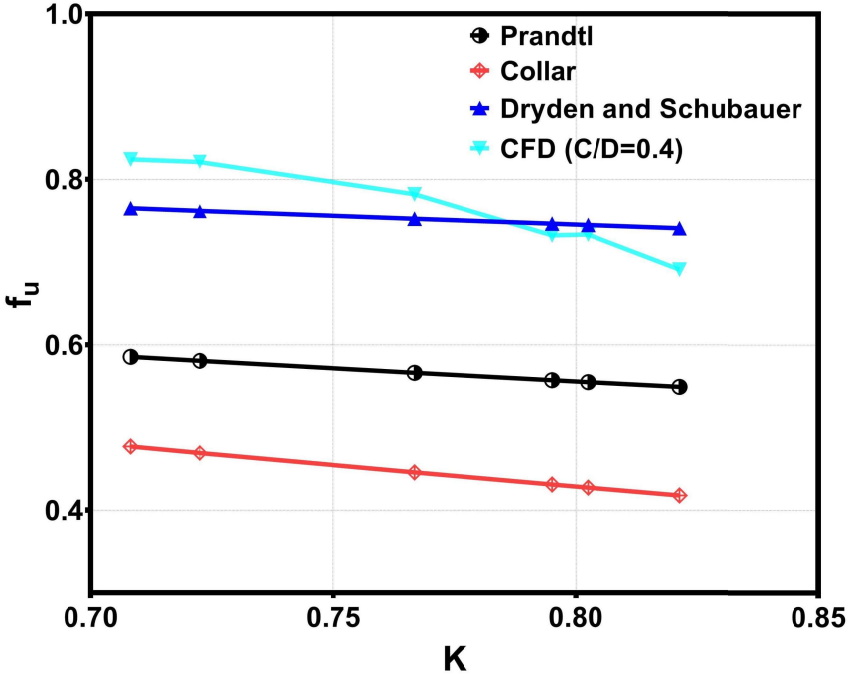

(d) screen sample 4

Response to Reviewer Comments

Manuscript title	Two Dimensional Simplification of Complex Three Dimensional Wire

Manuscript #	ASENG-3965

The authors wish to thank the editors and reviewers for their time in effort in reviewing our manuscript. We hope the changes listed have made the manuscript suit publication and we look forward to your response.

Editor Comments	Author's Response
t Reviewer #1 has some additional comments and questions. Please address the	time spent to examine the work in such detail. The comments from reviewer 2 is no

Reviewer 1's Comments	Author's Response
It is worth providing some quantitative comparison of computational resources required for 3D and 2D simulations to highlight the computational advantage of having a simplified model.	Computations were carried out on a single node-24 core grid platform, with a runtim 2D case taking an average of 120 mins, in contrast to 840 mins average runtime for t simulations. Therefore, 2D simulations were an average of 7 times faster than the 3D simulation cases. Simulation runtime comparison for 2D vs 3D cases is now introduce
of errors for mesh screen case 3 as compared to other cases? Since turbulence properties and flow fields are available from the simulation results, what can be identified to contribute to a higher percentage of error?	Results of the 3D and 2D cases all had a general trend of underpredicting flow loss co when compared to experiments, however the 2D mesh screen 3 case underpredicted more than the other screen cases, hence, screen 3 results gave higher percentage er compared to other screens. A possible reason for this is seen from the flow field resu

Reviewer 2's Comments	Author's Response

Reviewer 3's Comments	Author's Response

Thank you again for your time and effort, and for helping us improve the manuscript.

:able for

w addresse

ıe for each
he 3D
)
ed in Table
efficient
d slightly
ror when
ılts where

TABLE 2. Average Simulation Runtime

	2D Screen ($0 \leq \frac{C}{D} \leq 1$)	3D Screen
Sample 1	118.4 mins	841.2 mins
Sample 2	121.2 mins	836.5 mins
Sample 3	122.1 mins	844.1 mins
Sample 4	199.5 mins	839.4 mins

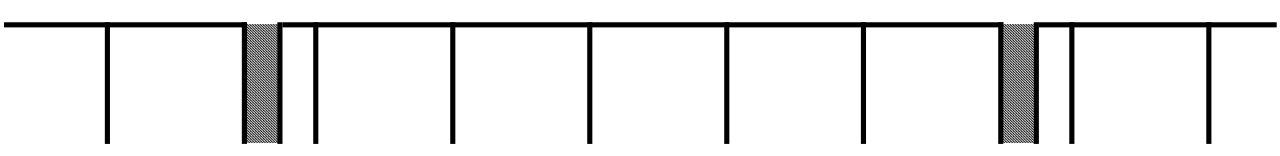

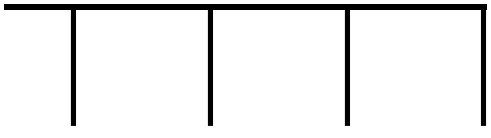

Response to Reviewer Comments Instructions

Please click on the red comments flag for more information

Manuscript title	

Manuscript #	

The authors wish to thank the editors and reviewers for their time in effort in reviewing our manuscript. We hope the changes listed have made the manuscrip for publication and we look forward to your response.

Editor Comments	Author's Response

Reviewer 1's Comments	Author's Response

Reviewer 2's Comments	Author's Response

Reviewer 3's Comments	Author's Response

Thank you again for your time and effort, and for helping us improve the manuscript.

ɔt suitable

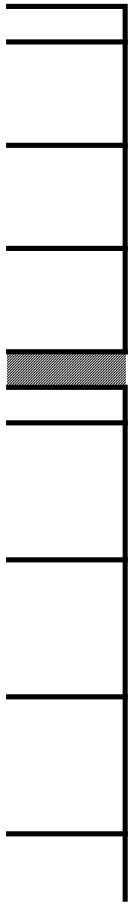

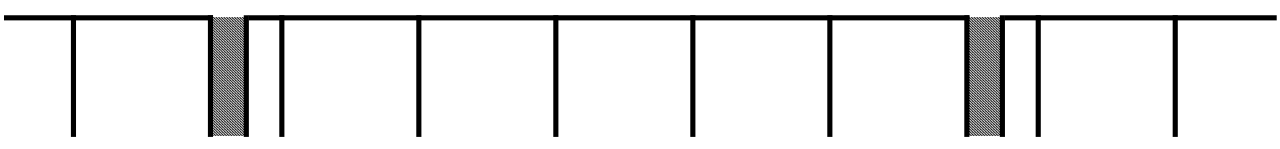

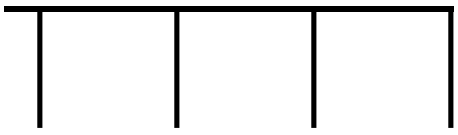

Responses to Reviewer 1 Comments.

Reviewer's comment No. 1

It is worth providing some quantitative comparison of computational resources required for 3D and 2D simulations to highlight the computational advantage of having a simplified model.

Authors Response:

Computations were carried out on a single node-24 core grid platform, with a runtime for each 2D case taking an average of 120 mins, in contrast to 840 mins average runtime for the 3D simulations. Therefore, 2D simulations were an average of 7 times faster than the 3D simulation cases.

Simulation runtime comparison for 2D vs 3D cases is now introduced in Table 2 of revised manuscript (shown below). This comment has now been updated in Line 190-193 of revised manuscript.

TABLE 2. Average Simulation Runtime

	2D Screen ($0 \leq \frac{C}{D} \leq 1$)	3D Screen
Sample 1	118.4 mins	841.2 mins
Sample 2	121.2 mins	836.5 mins
Sample 3	122.1 mins	844.1 mins
Sample 4	199.5 mins	839.4 mins

Table 2

Reviewer's comment No. 2

Can the authors please comment on the possible causes of larger percentage of errors for mesh screen case 3 as compared to other cases? Since turbulence properties and flow fields are available from the simulation results, what can be identified to contribute to a higher percentage of error?

Authors Response:

Results of the 3D and 2D cases all had a general trend of underpredicting flow loss coefficient when compared to experiments, however the 2D mesh screen 3 case underpredicted slightly more than the other screen cases, hence, screen 3 results gave higher percentage error when compared to other screens. A possible reason for this is seen from the flow field results where mesh screen 3 showed to slightly underpredict particularly more pressure loss and turbulence kinetic energy when compared to other screen cases. The underprediction of screen 3 when compared to other 2D screen cases did not have a correlated trend with their screen geometric features (e.g, screen diameter, streamwise & spanwise pitch, porosity, or solidity).

This comment has now been updated in Line 370-377 of revised manuscript.